THE UNIVERSITY of EDINBURGH

Edinburgh Research Explorer

Argon redistribution during a metamorphic cycle: Consequences for determining cooling rates

Citation for published version:
Kelley, S, McDonald, C, Mark, D, Warren, C, Halton, A & Sherlock, S 2016, 'Argon redistribution during a metamorphic cycle: Consequences for determining cooling rates', *Chemical Geology*, vol. 443, pp. 182-197. https://doi.org/10.1016/j.chemgeo.2016.09.028

Digital Object Identifier (DOI):
10.1016/j.chemgeo.2016.09.028

Link:
Link to publication record in Edinburgh Research Explorer

Document Version:
Publisher's PDF, also known as Version of record

Published In:
Chemical Geology

General rights
Copyright for the publications made accessible via the Edinburgh Research Explorer is retained by the author(s) and / or other copyright owners and it is a condition of accessing these publications that users recognise and abide by the legal requirements associated with these rights.

Take down policy
The University of Edinburgh has made every reasonable effort to ensure that Edinburgh Research Explorer content complies with UK legislation. If you believe that the public display of this file breaches copyright please contact openaccess@ed.ac.uk providing details, and we will remove access to the work immediately and investigate your claim.

Download date: 05. May. 2023

Chemical Geology 443 (2016) 182–197

Contents lists available at ScienceDirect

Chemical Geology

journal homepage: www.elsevier.com/locate/chemgeo

Argon redistribution during a metamorphic cycle: Consequences for determining cooling rates

Christopher S. McDonald [a,b], Clare J. Warren [a,*], Darren F. Mark [c], Alison M. Halton [d], Simon P. Kelley [a], Sarah C. Sherlock [d]

[a] School of Environment, Earth and Ecosystem Sciences, The Open University, Walton Hall, Milton Keynes, MK7 6AA, United Kingdom
[b] School for Earth and Space Exploration, Arizona State University, BOX 876004, Tempe, AZ 85287-6004, United States
[c] Scottish Universities Environment Research Centre, Rankine Avenue, Scottish Enterprise Technology Park, East Kilbride, Scotland, G75 0QF, United Kingdom
[d] School of Physical Sciences, The Open University, Walton Hall, Milton Keynes MK7 6AA, United Kingdom

ARTICLE INFO

Article history:
Received 15 May 2016
Received in revised form 20 September 2016
Accepted 21 September 2016
Available online 23 September 2016

Keywords:
$^{40}Ar/^{39}Ar$ thermochronology
Western Gneiss Region
Metamorphism
Exhumation
Cooling rates

ABSTRACT

$^{40}Ar/^{39}Ar$ thermochronology is commonly used to constrain the rates and times of cooling in exhumed metamorphic terranes, with ages usually linked to temperature via Dodson's closure temperature (T_C) formulation. Whilst many metamorphic $^{40}Ar/^{39}Ar$ data are consistent with the timing of crystallisation or cooling within a chronological framework defined by other, higher temperature, chronometers, other $^{40}Ar/^{39}Ar$ data are more difficult to interpret. We report white mica and biotite single grain fusion and laser ablation $^{40}Ar/^{39}Ar$ ages from felsic gneisses from the Western Gneiss Region, Norway. The rocks record isothermal decompression from peak eclogite-facies conditions (white mica stable) to amphibolite-facies conditions (biotite stable) at c. 700 °C. White mica and biotite yield dispersed single grain fusion dates from 416 to 373 Ma and 437 to 360 Ma respectively. In-situ laser ablation analyses provide a similar range, with white mica spot ages ranging from 424 to 370 Ma and biotite spot ages ranging from 437 to 370 Ma. The dates span the duration of the metamorphic cycle suggested by previous studies, and cannot be reconciled with the results of simple models of Ar loss by diffusion during cooling. Samples that show evidence for different physical processes, such as the chemical breakdown of white mica, partial melting, and fluid ingress, generated different age populations to samples that did not experience or record obvious petrological evidence for these processes. Samples that record significant recrystallization and deformation yielded younger white mica (but older biotite) single grain fusion ages than more pristine samples. Amphibolite-facies gneisses that preserve evidence for significant partial melting generated younger biotite ages than samples that recorded evidence for significant hydration. Our data support other reported observations that high-temperature metamorphic mica $^{40}Ar/^{39}Ar$ dates cannot be assumed to record the timing of cooling through a specific temperature window. Careful assessment of the petrographic context of the dated minerals and consideration of their post-crystallisation history may provide a more robust insight into whether 'age' links to 'stage' in a temporally meaningful way.

© 2016 The Authors. Published by Elsevier B.V. This is an open access article under the CC BY license (http://creativecommons.org/licenses/by/4.0/).

1. Introduction

Understanding the timing of when, and the rate at which, metamorphic terranes are exhumed through the Earth's mantle and crust is important for constraining geodynamic models of tectonic processes. $^{40}Ar/^{39}Ar$ mica thermochronology is typically employed to constrain exhumation and cooling rates, with age most commonly being linked to temperature via the Dodson closure temperature (T_C) formulation (Dodson, 1973). This solution to the diffusion equation is only applicable for geological applications under the following boundary conditions: (1) negligible initial lattice-hosted ^{40}Ar during crystallisation (i.e. a very low mineral:fluid partition coefficient), (2) Ar distribution within the mineral controlled only by thermally-activated volume diffusion that adheres to Fick's 2nd law of diffusion (modified for a source term), (3) an 'open' grain boundary network (i.e. the grain boundary effectively has a negligible concentration of Ar) during the temperature interval over which within-grain Ar diffusion is efficient and (4) initial crystallisation at a temperature at which within-grain Ar diffusion is efficient.

As geochronological data continues to be collected at ever-higher spatial resolution and analytical precision, it is becoming possible to test some, but not all, of the listed boundary conditions. This is important for determining the geological scenarios in which the Dodson T_C formulation is justifiably applicable vs. those situations where it is not. For example mineral thermobarometers provide estimates of

* Corresponding author.
E-mail address: clare.warren@open.ac.uk (C.J. Warren).

http://dx.doi.org/10.1016/j.chemgeo.2016.09.028
0009-2541/© 2016 The Authors. Published by Elsevier B.V. This is an open access article under the CC BY license (http://creativecommons.org/licenses/by/4.0/).

metamorphic pressure-temperature conditions at different stages of the rock evolution, which, when coupled to experimental diffusion parameters, provide insight into whether a specific rock reached temperatures high enough for efficient diffusion in different minerals (c.f. Warren et al., 2012c). In-situ laser ablation profiles across grains of sufficient size can provide evidence for diffusion (e.g. Wartho and Kelley, 2003). Petrological modelling and a temporal framework based on independent higher-temperature chronometers coupled with diffusion modelling provide a solid platform for assessing open system behaviour and/or incorporation of initial ^{40}Ar during crystallisation.

Over the last few decades, a significant number of studies have shown that micas in high pressure (>15 kbar) metamorphic rocks appear to be particularly prone to yielding $^{40}Ar/^{39}Ar$ ages that are "too old" relative to other independently constrained 'events' along their *P-T* paths. For example, despite temperatures high enough for theoretically effective diffusion, $^{40}Ar/^{39}Ar$ data from high pressure micas commonly produce ages that are older than the timing of peak metamorphism from zircon U-Pb data, or relative to the petrographically-constrained timing of mica crystallisation, (Foland, 1979; Li et al., 1994; Arnaud and Kelley, 1995; Scaillet, 1996; Ruffet et al., 1997; Sherlock and Arnaud, 1999; Baxter et al., 2002; Warren et al., 2012a). Studies suggest that the incorporation of "excess" ^{40}Ar ($^{40}Ar_E$, decoupled from its parent ^{40}K) by diffusion from the grain boundary into the mineral lattice and/or lattice defects, or during deformation or (re)crystallisation may modify ^{40}Ar concentrations (Li et al., 1994; Ruffet et al., 1997; Pickles et al., 1997; Villa, 1998; Sherlock and Kelley, 2002; Wartho and Kelley, 2003; Di Vincenzo, 2004; Warren et al., 2011). Other studies suggest that non-zero grain boundary conditions were experienced during or after crystallisation: high Ar concentrations in the grain boundary would hinder efficient diffusive loss of Ar, and lead to inherited ages that are older than predicted by the Dodson T_C formulation, but younger than the timing of mineral crystallisation (c.f. Baxter et al., 2002). Recent experimental data additionally suggest that Ar diffusion in white mica is pressure- as well as temperature-dependent (Harrison et al., 2009), suggesting higher Ar retention than previously suspected at metamorphic pressures >10 kbar.

$^{40}Ar/^{39}Ar$ data may therefore relate to the timing of mineral crystallisation, the timing of cooling through a specific temperature or temperature interval (specifically whether they adhere to the Dodson T_C formulation), or may be geologically meaningless. Determining between these options is important for quantifying rates and timescales of tectonic processes. Here we track the incorporation, release, and transport of Ar within and between different minerals during a metamorphic cycle, and especially during the exhumation-related, retrograde metamorphic reactions. The study of such processes informs the assessment of the main mechanism(s) for redistributing Ar within minerals, and provides example cases for which $^{40}Ar/^{39}Ar$ may or may not be reliably linked to temperature via the Dodson T_C formulation.

Mid- to lower-crustal felsic gneisses exposed in the Western Gneiss Region (WGR), western Norway provide an excellent natural laboratory for determining Ar behaviour during a burial-exhumation cycle because the gneisses are broadly similar in composition but preserve different stages of the metamorphic evolution. The WGR experienced a high temperature evolution (~700 °C) for 10–15 Ma (Wain et al., 2000, Hacker, 2007, Spencer et al., 2013, Kylander-Clark & Kylander-Clark and Hacker, 2014) – long enough for diffusive processes to have been, in theory, efficient enough for all micas of the same grain size and composition to retain the same $^{40}Ar/^{39}Ar$ age (Warren et al., 2012b). Published white mica $^{40}Ar/^{39}Ar$ multi- and single-grain step heating ages from the Outer Nordfjord area range from 409 to 380 Ma and are interpreted as cooling ages (Root et al., 2005; Young et al., 2011). Published white mica and biotite $^{40}Ar/^{39}Ar$ multi- and single-grain step heating ages from the Outer Nordfjord area range from 389 to 374 Ma and 402 to 375 Ma, respectively, and interpreted as cooling ages (Lux, 1985; Berry et al., 1995; Hacker and Gans, 2005; Root et al., 2005; Walsh et al., 2007; Young et al., 2011; Walsh et al., 2013). More recent single grain fusion and in-situ laser ablation techniques have yielded highly variable white mica $^{40}Ar/^{39}Ar$ ages, both within and between grains in the same sample, as well as between different samples (Warren et al., 2012a). The range generated by the single grain fusion data was greater than the range expected from diffusive loss in different grain sizes. Furthermore, the spatial patterns that the in-situ data showed were inconsistent with diffusive loss on cooling.

Here we systematically document age populations from samples that show evidence for different physical processes including mineral breakdown/replacement, deformation, partial melting, and hydration, and compare them with age populations from samples that have not experienced or recorded evidence for these processes. Our data show that all samples generate a range of $^{40}Ar/^{39}Ar$ ages spanning at least 15 Ma. Samples that preserve evidence for significant recrystallization and deformation displayed younger white mica, but older biotite, single grain fusion age populations than more pristine samples. Amphibolite-facies gneisses preserving evidence for significant partial melting yield younger biotite

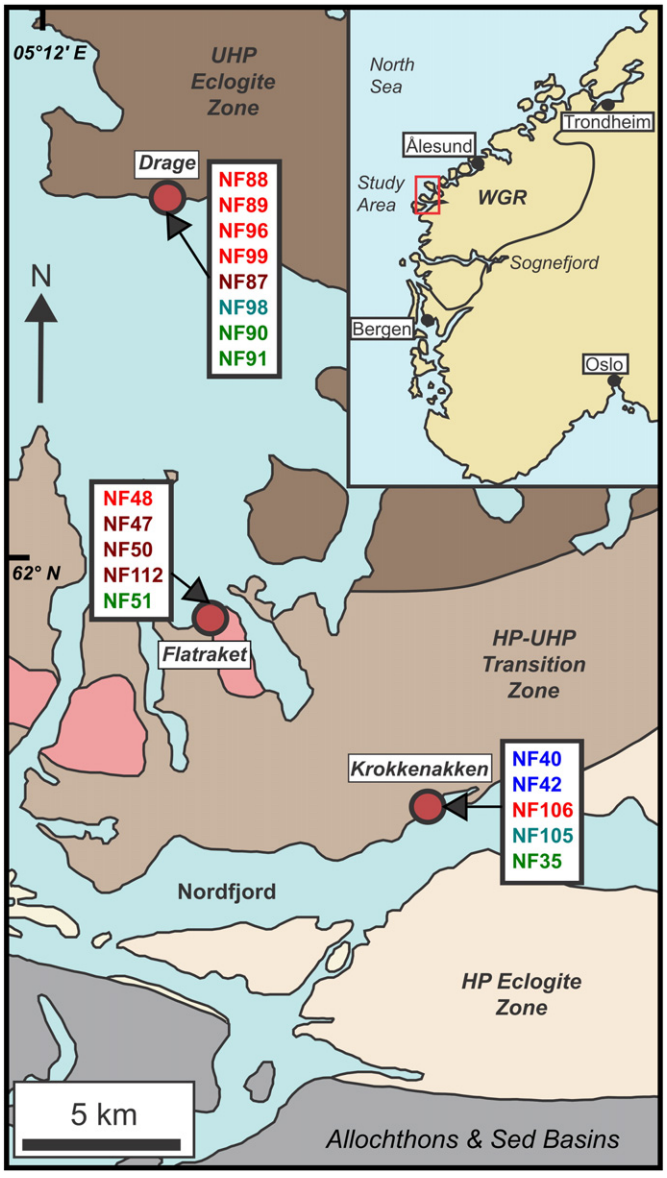

Fig. 1. A simplified geological map, modified after Wain (1997), of the Outer Nordfjord region of the Western Gneiss Region (WGR), Norway, showing the locations of the study sites and the sample numbers collected from each locality. The sample numbers are colour-coded to reflect the petrological groups defined in the text. Blue = Group 1a; Red = Group 1b; Brown = Group 1c; Teal = Group 2a; and Green = Group 2b. UHP = ultra-high pressure; HP = high pressure.

Table 1
White mica data.

Gneiss group	1A						1B												2A			
Sample	NF40		NF42		NF43		NF106		NF48		NF88		NF89		NF96		NF99		NF98		NF105	
Position	Core	Rim	Core	Rim	Core	Rim	Core	Rim	Core	Rim	Core	Rim	Core	Rim	Core	Rim	Core	Rim	Core	Rim	Core	Rim
SiO_2	50.24	49.08	49.68	48.86	50.25	48.80	47.75	43.72	48.86	46.60	47.12	45.88	47.09	46.16	47.98	45.57	49.65	45.31	47.63	46.04	48.05	47.80
TiO_2	0.33	0.56	0.19	0.41	0.30	0.38	0.40	0.59	0.73	0.91	1.20	1.12	1.13	0.74	1.19	0.90	0.86	0.42	1.23	0.94	0.87	0.86
Al_2O_3	28.41	29.72	27.32	29.00	26.73	28.14	28.19	32.96	29.28	31.17	30.65	32.55	30.61	32.00	30.00	32.69	28.40	32.56	28.12	30.13	26.70	27.16
Cr_2O_3	0.02	0.01	0.02	0.03	0.07	0.07	0.03	0.00	0.01	0.02	0.00	0.00	0.01	0.02	0.04	0.03	0.01	0.00	0.02	0.00	0.00	0.03
FeO	2.66	2.72	1.99	1.81	2.68	2.69	2.95	2.85	2.51	2.67	2.22	1.99	2.71	2.70	2.84	2.50	2.68	2.71	4.34	4.23	4.56	4.55
MnO	0.01	0.00	0.02	0.00	0.02	0.00	0.01	0.00	0.00	0.00	0.02	0.01	0.02	0.03	0.04	0.00	0.01	0.02	0.02	0.00	0.02	0.03
MgO	2.58	2.16	3.68	3.04	3.29	2.74	2.62	1.06	1.98	1.38	1.64	1.03	1.38	1.05	1.78	0.85	2.32	0.97	1.90	1.33	2.17	2.16
CaO	0.00	0.00	0.01	0.00	0.00	0.02	0.00	0.01	0.00	0.05	0.01	0.01	0.01	0.00	0.01	0.01	0.02	0.03	0.00	0.01	0.00	0.00
Na_2O	0.67	0.75	0.39	0.41	0.20	0.17	0.32	0.46	0.53	0.63	0.46	0.54	0.35	0.37	0.52	0.53	0.36	0.52	0.22	0.25	0.22	0.22
K_2O	9.44	9.70	9.59	9.92	10.41	10.59	10.29	10.32	9.90	9.89	10.33	10.45	10.54	10.81	10.53	10.51	10.22	10.41	10.81	10.78	10.79	10.82
F	0.22	0.14	0.05	0.02	0.10	0.08	0.00	0.00	0.07	0.15	0.10	0.00	0.05	0.10	0.12	0.00	0.11	0.00	0.04	0.10	0.07	0.09
Cl	0.00	0.01	0.00	0.01	0.00	0.00	0.01	0.00	0.00	0.00	0.01	0.00	0.00	0.00	0.01	0.01	0.00	0.01	0.01	0.00	0.01	0.00
Total	94.58	94.88	93.00	93.49	94.07	93.68	92.58	91.97	93.89	93.48	93.76	93.58	93.93	93.98	95.06	93.61	94.64	92.96	94.34	93.80	93.46	93.72
Ions per 22 O																						
Si	6.75	6.59	6.77	6.62	6.82	6.66	6.60	6.11	6.62	6.38	6.42	6.25	6.42	6.31	6.48	6.23	6.69	6.24	6.53	6.36	6.66	6.62
Ti	0.03	0.06	0.02	0.04	0.03	0.04	0.04	0.06	0.07	0.09	0.12	0.12	0.12	0.08	0.12	0.09	0.09	0.04	0.13	0.10	0.09	0.09
Al	4.50	4.71	4.38	4.63	4.27	4.53	4.59	5.42	4.68	5.03	4.92	5.23	4.92	5.15	4.77	5.27	4.51	5.29	4.55	4.91	4.36	4.43
Cr	0.00	0.00	0.00	0.01	0.01	0.01	0.01	0.00	0.00	0.00	0.00	0.00	0.00	0.00	0.01	0.01	0.00	0.00	0.00	0.00	0.00	0.01
Fe	0.30	0.31	0.23	0.20	0.30	0.31	0.34	0.33	0.29	0.30	0.25	0.23	0.31	0.31	0.32	0.29	0.30	0.31	0.50	0.49	0.53	0.53
Mn	0.00	0.00	0.01	0.00	0.00	0.00	0.00	0.00	0.00	0.00	0.00	0.00	0.01	0.01	0.01	0.00	0.00	0.00	0.00	0.00	0.00	0.01
Mg	0.52	0.43	0.75	0.62	0.67	0.56	0.54	0.22	0.40	0.28	0.34	0.21	0.28	0.21	0.36	0.18	0.47	0.20	0.39	0.28	0.45	0.45
Ca	0.00	0.00	0.00	0.00	0.00	0.01	0.00	0.00	0.00	0.01	0.00	0.00	0.00	0.00	0.00	0.00	0.00	0.01	0.00	0.00	0.00	0.00
Na	0.18	0.19	0.10	0.11	0.05	0.04	0.09	0.13	0.14	0.17	0.12	0.14	0.09	0.10	0.14	0.14	0.09	0.14	0.06	0.07	0.06	0.06
K	1.62	1.66	1.67	1.72	1.80	1.84	1.82	1.84	1.71	1.73	1.79	1.82	1.83	1.89	1.82	1.83	1.75	1.83	1.89	1.90	1.91	1.91
F	0.09	0.06	0.02	0.01	0.04	0.03	0.00	0.00	0.03	0.07	0.04	0.00	0.02	0.04	0.05	0.00	0.04	0.00	0.02	0.04	0.03	0.04
Cl	0.00	0.00	0.00	0.00	0.00	0.00	0.00	0.00	0.00	0.00	0.00	0.00	0.00	0.00	0.00	0.00	0.00	0.00	0.00	0.00	0.00	0.00
Total	14.00	14.01	13.94	13.95	14.00	14.03	14.02	14.11	13.94	14.05	14.02	14.00	14.00	14.09	14.06	14.03	13.96	14.06	14.07	14.14	14.10	14.12

ages than samples that record evidence for fluid infiltration during the amphibolite-facies overprint. Overall our results show that most of the $^{40}Ar/^{39}Ar$ mica dates from the WGR are inconsistent with the interpretation that they record the time at which the rock cooled through a fixed temperature interval. Instead the ^{40}Ar concentrations appear to trace other physical processes that affected the rocks during exhumation.

1.1. Regional geology

The Western Gneiss Region (WGR) exposed in western Norway is a 50,000 km^2 basement window within the Scandinavian Caledonides, formed during the subduction of the leading edge of Baltica beneath Laurentia during the Scandian Phase of the Caledonian Orogeny (Gee, 1975; Roberts, 2003; Hacker, 2007). The dominant lithology in the WGR is amphibolite-facies felsic gneiss, with local eclogite enclaves (Eskola, 1921; Bryhni, 1966). Evidence for ultrahigh-pressure metamorphism (UHP; >2.6 GPa) is preserved across c. 5000 km^2 of the WGR (Smith, 1984; Root et al., 2005). Coesite (the high pressure polymorph of quartz whose presence confirms that UHP conditions were reached) has been documented mostly within eclogite, but rare occurrences have also been documented in the felsic host gneisses (Wain, 1997). There are three confirmed UHP domains: the Nordfjord-Stadlandet (southernmost), the Sorøyane (central) and the Nordøyane (northern). This study focuses on the Nordfjord-Stadlandet domain, where the recorded/preserved P-T gradient ranges from quartz eclogite-facies in the southeast (~2.5 GPa and ~600 °C) to coesite-stable eclogite-facies in the northwest (~3.0 GPa and ~700 °C) across 2500 km^2 (Labrousse et al., 2004; Root et al., 2005; Young et al., 2007). Following near-isothermal decompression from (U)HP conditions, the entire WGR experienced retrograde amphibolite-facies metamorphism at ~700 °C and 1 GPa (Walsh and Hacker, 2004).

Multiple radioisotopic dating techniques provide an independent temporal framework constraining the timing of peak metamorphism and exhumation across the Outer Nordfjord Region. Sm-Nd and Lu-Hf garnet ages suggest prograde metamorphism and burial from c. 440 Ma to c. 404 Ma (Griffin and Brueckner, 1980; Mearns, 1986; Carswell et al., 2003; Kylander-Clark et al., 2007; Peterman et al., 2009). U-Pb zircon ages in mafic eclogite bodies suggest that peak eclogite-facies metamorphic conditions were achieved by c. 410–400 Ma (Root et al., 2004, Young et al., 2007, Kylander-Clark and Hacker, 2014, Young and Kylander-Clark, 2015). U-Pb titanite ages of c. 399 to 379 Ma from the Nordfjord area suggest host gneiss recrystallization under amphibolite-facies conditions during exhumation (Spencer et al., 2013), and U-Pb zircon ages from an undeformed granitic pegmatite dyke suggest post-eclogite-facies partial melting and crystallisation at c. 389 Ma (Kylander-Clark and Hacker, 2014).

1.2. Study sites

Samples were collected from Krokkenakken, Flatraket Harbour and Drage in the Outer Nordfjord area (Fig. 1). These localities expose variably-amphibolitised eclogite-facies mafic rocks hosted in felsic gneisses. Each locality preserves evidence for different peak metamorphic conditions, ranging from ~600 °C at 2.3 GPa at Krokkenakken to ~750 °C at 3.2 GPa at Drage (Cuthbert et al., 2000). All locations record similar amphibolite-facies conditions of ~700 °C and 1 GPa (e.g. Krabbendam and Wain, 1997; Labrousse et al., 2004).

The felsic gneisses record different stages along the retrograde metamorphic path: garnet-bearing gneisses, located within strain shadows adjacent to the mafic boudins, preserve relicts of the HP history (e.g. symplectites after omphacite) whereas biotite-epidote gneisses, located further from the mafic units, only record mid-crustal amphibolite-facies conditions.

2. Petrology and mineral chemistry

Major-element compositions of white mica and biotite were analysed using the Open University Cameca SX-100 electron microprobe using a spot size of 10 μm, conditions of 15 kV, 20 nA and 30 s collection time. Calibrations were performed on natural standards, and analyses were corrected using a ZAF matrix correction routine. Analyses were bracketed by analyses of secondary standards to check for major element reproducibility of 1%. Average white mica and biotite compositions are reported in Tables 1 and 2 respectively; full data are reported in Supplementary Table S.1.

The felsic gneisses form two petrographically-distinct groups: garnet-bearing gneisses that record exhumation from eclogite-facies conditions (Group 1, Fig. 2A) and biotite-epidote gneisses that record the amphibolite-facies overprint (Group 2, Fig. 2B and C; a full petrographic description of each sample is provided in Supplementary material S.2). Major element XRF data suggest similar bulk compositions for these different groups (Young and Kylander-Clark, 2015).

The garnet-bearing (Group 1) gneisses comprise three sub-groups: those that still preserve HP relicts (Group 1a), those that lack HP minerals but still contain white mica, albeit heavily replaced by biotite-plagioclase symplectites (Group 1b) and those that lack HP relicts and no longer contain white mica (although do preserve symplectites indicative of the former presence of white mica; Group 1c).

Group 1a gneisses are found in a low-strain region adjacent to a large (>300 m long) eclogite boudin at Krokkenakken (samples NF40, NF42, and NF43; Fig. 2D). They are medium-grained, unfoliated gneisses with a peak assemblage of quartz, white mica and garnet with accessory apatite, rutile, zircon, clinozoisite, and kyanite. Symplectites of clinopyroxene and plagioclase provide evidence for precursor omphacite (Wain et al., 2000). White micas are 0.5–2.5 mm in length, with Si ranging from 6.8 per 22 oxygens per formula unit (pfu) in the cores to 6.3 pfu in the rims. White mica is commonly almost completely replaced by biotite-plagioclase symplectites at the rims. Biotite grains within the symplectite are generally <0.5 mm in size and are chemically variable with Mg/Mg + Fe (Mg#) of 0.52–0.73 and Ti concentrations of 0.2–0.3 pfu.

Group 1b gneisses occur at all three localities (Krokkenakken: NF106; Flatraket Harbour: NF48; Fig. 2E) and Drage: NF88, NF89, NF96 and NF99). These gneisses are foliated and composed of quartz, plagioclase feldspar, garnet, white mica, biotite, and rare alkali feldspar with accessory rutile, apatite, and zircon. White micas, 0.5–2.5 mm in length, are zoned in Si from 6.8 pfu in the core to 6.1 pfu in the rim. Narrow 0.5–1 μm wide rims are altered to biotite + plagioclase symplectite. Biotite grains <0.5 mm in length also forms fabric-defining euhedral laths. These grains show a wide range in composition with Mg# ranging from 0.46–0.51 and Ti concentrations between 0.23 and 0.34 pfu from core to rim.

Subordinate in volume to Group 1b gneisses, Group 1c gneisses preserve neither HP mineral relicts nor white mica (Flatraket Harbour: NF47, NF50 and NF112; Drage: NF87). These gneisses are located close to the contact with the mafic eclogites and are also found close to the contact with the amphibolite-facies biotite-epidote gneisses described below. They contain quartz, plagioclase feldspar, garnet, epidote (commonly with allanite cores), and biotite with accessory rutile, apatite, and zircon. Rare biotite-plagioclase symplectites preserved in quartz ribbons attest to the former presence of white mica (Fig. 2F). Further biotite laths are generally <1 mm in length and yield a narrow range in composition with Mg# values from 0.53–0.58 and Ti concentrations from 0.20–0.34 pfu.

Group 2 biotite-epidote gneisses form approximately 70% by volume of the felsic gneisses in the study area (e.g. Peterman et al., 2009). They are typically foliated and preserve the lowest metamorphic grade assemblages. At Drage (Fig. 1), within the core of the antiformal Nordfjord-Stadlandet UHP domain, Group 2 gneisses are intensely migmatised.

Table 2
Biotite data.

Gneiss group	1A						1B											
Sample	NF40		NF42		NF43		NF106		NF48		NF88		NF89		NF96		NF99	
Position	Core	Rim	Core	Rim	Core	Rim	Core	Rim	Core	Rim	Core	Rim	Core	Rim	Core	Rim	Core	Rim
SiO_2	37.13	36.73	37.85	37.65	35.81	35.74	36.26	36.78	35.76	36.07	35.98	35.80	35.83	36.05	36.09	34.73	35.96	35.12
TiO_2	1.89	1.95	2.27	2.22	2.64	2.70	2.93	3.28	2.43	2.35	2.64	2.50	3.02	2.87	2.74	2.57	2.34	2.51
Al_2O_3	17.94	17.90	16.95	17.40	18.52	18.64	16.70	16.41	17.73	17.88	17.84	18.35	17.82	17.91	17.85	17.81	17.90	17.96
Cr_2O_3	0.04	0.03	0.03	0.02	0.04	0.05	0.02	0.01	0.02	0.00	0.02	0.01	0.04	0.04	0.04	0.03	0.00	0.03
FeO	15.54	15.36	12.96	12.59	17.21	17.38	18.38	17.95	18.22	18.22	20.20	19.81	19.52	19.27	18.95	19.07	19.45	20.42
MnO	0.07	0.05	0.03	0.03	0.17	0.16	0.16	0.17	0.14	0.15	0.16	0.20	0.36	0.39	0.22	0.22	0.18	0.20
MgO	12.58	12.43	15.37	15.63	10.61	10.64	11.32	11.47	10.62	10.69	9.36	9.37	9.25	9.27	10.41	11.00	9.96	9.76
CaO	0.13	0.06	0.03	0.08	0.00	0.00	0.06	0.01	0.02	0.02	0.01	0.05	0.00	0.02	0.00	0.02	0.02	0.05
Na_2O	0.27	0.25	0.15	0.10	0.13	0.09	0.08	0.09	0.14	0.10	0.11	0.10	0.13	0.10	0.07	0.06	0.11	0.09
K_2O	8.61	8.92	9.07	8.76	9.53	9.46	8.84	9.34	9.18	9.31	9.44	9.39	9.59	9.60	9.59	8.57	9.54	8.96
F	0.14	0.22	0.12	0.15	0.10	0.02	0.14	0.21	0.13	0.13	0.09	0.12	0.00	0.18	0.24	0.11	0.12	0.08
Cl	0.01	0.01	0.00	0.00	0.00	0.00	0.01	0.02	0.04	0.03	0.03	0.03	0.05	0.05	0.06	0.05	0.04	0.08
Total	94.43	93.98	94.93	94.68	94.81	94.92	94.90	95.74	94.48	94.96	95.87	95.74	95.60	95.75	96.25	94.24	95.60	95.26
Ions per 22 O																		
Si	5.58	5.57	5.60	5.57	5.44	5.42	5.52	5.56	5.48	5.49	5.48	5.45	5.46	5.49	5.47	5.35	5.48	5.40
Ti	0.21	0.22	0.25	0.25	0.30	0.31	0.34	0.37	0.28	0.27	0.30	0.29	0.35	0.33	0.31	0.30	0.27	0.29
Al	3.18	3.20	2.95	3.03	3.32	3.33	3.00	2.93	3.20	3.21	3.20	3.29	3.20	3.22	3.18	3.23	3.22	3.25
Cr	0.01	0.01	0.01	0.00	0.01	0.01	0.00	0.00	0.00	0.00	0.01	0.00	0.01	0.01	0.01	0.01	0.00	0.01
Fe	1.95	1.95	1.61	1.56	2.19	2.21	2.34	2.27	2.34	2.32	2.57	2.52	2.49	2.46	2.40	2.46	2.48	2.62
Mn	0.01	0.01	0.01	0.01	0.02	0.02	0.02	0.02	0.02	0.02	0.02	0.03	0.04	0.05	0.03	0.03	0.02	0.03
Mg	2.82	2.81	3.39	3.44	2.40	2.40	2.57	2.59	2.43	2.43	2.12	2.13	2.10	2.11	2.35	2.53	2.26	2.23
Ca	0.02	0.01	0.01	0.01	0.00	0.00	0.01	0.00	0.01	0.00	0.00	0.01	0.00	0.01	0.00	0.00	0.01	0.01
Na	0.08	0.08	0.04	0.03	0.04	0.03	0.02	0.03	0.04	0.03	0.03	0.03	0.04	0.03	0.02	0.02	0.03	0.03
K	1.65	1.72	1.71	1.65	1.85	1.83	1.72	1.80	1.79	1.81	1.83	1.83	1.86	1.87	1.85	1.69	1.85	1.75
F	0.07	0.10	0.06	0.07	0.05	0.01	0.07	0.10	0.07	0.07	0.04	0.06	0.00	0.09	0.12	0.06	0.06	0.04
Cl	0.00	0.01	0.00	0.00	0.00	0.00	0.01	0.01	0.01	0.01	0.01	0.01	0.01	0.01	0.02	0.01	0.01	0.02
Total	15.58	15.68	15.64	15.61	15.61	15.55	15.61	15.68	15.67	15.65	15.63	15.64	15.56	15.66	15.75	15.68	15.69	15.67

Group 2a gneisses preserve relict white mica, whereas Group 2b do not. Group 2a are located close to the contact with Group 1c and contain an amphibolite-facies assemblage of biotite, epidote, quartz and plagioclase. They also commonly preserve skeletal relicts of white mica and garnet (Fig. 2D). The white mica shows evidence of melting, being replaced by alkali feldspar + quartz at their rims. This type of gneiss occurs only at Krokkenakken (NF105) and at Drage (NF98; Fig. 2G). Relict white mica grains are <0.5 mm in length and zoned in Si (6.6–6.3 pfu from core to rim). The biotite grains are 0.5–1 mm in length and form subhedral to euhedral laths that define the fabric. Biotite preserves a broad range of compositions with Mg# ranging from 0.40–0.51 and Ti concentrations from 0.12–0.42 pfu.

Group 2b samples include NF35 from Krokkenakken, NF51 from Flatraket Harbour (Fig. 2H) and samples NF90 and NF91 from Drage. They contain quartz, plagioclase, biotite, epidote (with common allanite cores and forming prominent porphyroblasts), minor amphibole, and K-feldspar. Accessory phases include titanite, ilmenite, apatite, and zircon. Biotite defines the fabric and is often inter-grown with titanite. The fabric both wraps around and is overprinted by the epidote porphyroblasts, suggesting epidote growth both during and after amphibolite-facies conditions (Fig. 2H). Biotite grains are ~1 mm in length and preserve a broad range in chemistry, with Mg# varying from 0.37 to 0.55 and with Ti concentrations from 0.20 to 0.37 pfu.

3. $^{40}Ar/^{39}Ar$ analyses

19 samples were selected for single grain fusion analysis to determine the presence of any age variations within and between different samples. For single grain fusion analysis, ~50 grains of white mica and biotite were picked from each crushed sample. Grains showing the least deformation and the fewest inclusions were selected. Care was taken to avoid picking white mica grains rimmed by biotite-plagioclase symplectites. Grains were washed in acetone or methanol and distilled water before being packed into aluminium foil packets. Polished thick sections (~250 μm) for in-situ laser ablation analysis were prepared by adhesion to glass slides with cyanoacrylate ("super glue"). Sections were removed from the glass by soaking in acetone for up to 24 h to dissolve the glue, and then cut into 5 × 5 mm squares before washing and packing as above.

Samples were analysed at two facilities: the $^{40}Ar/^{39}Ar$ and Noble Gas Laboratory at the Open University (OU), and the NERC-funded Argon Isotope Facility (AIF) housed at the Scottish Universities Environmental Research Centre (SUERC). Analytical details are summarised below; full details are provided in Supplementary document S.3. Two mass spectrometers were used at the OU. Total fusion of single grains of the unknowns and flux monitors was achieved using a 1062 nm CSI Fibre laser coupled to an automated gas handling vacuum system and admitted to a MAP 215-50 noble gas mass spectrometer (Warren et al., 2012a). Samples were fused over 60–90 s and gasses cleaned for 210 s through two SAES AP10 Zr-Al getters (one at room temperature and the other at 450 °C). A liquid nitrogen cold trap provided additional gas cleaning prior to inlet to the mass spectrometer.

High spatial resolution single spot and traverse analyses on polished thick sections were achieved using a New Wave Systems Nd-YAG 213 nm ultraviolet (UV) laser coupled to a Nu Instruments Noblesse gas mass spectrometer (Sherlock et al., 2005). UV analyses consisted of ablating 30 μm diameter spots for 90 s, at 20 Hz and an on-sample fluence of 3.8 mJ cm^{-2}. Gasses were subsequently cleaned for 90 s through two SAES AP10 Zr-Al getters (one at room temperature and the other at 450 °C).

At SUERC, single grain fusions were achieved using a Merchantek 25 W CO_2 laser coupled to a GVI ARGUS multi-collector mass spectrometer (Mark et al., 2009; Mark et al., 2011). Samples were fused over 20 s prior to 300 s gas clean-up using two GP50 SAES getters (one at room temperature and the other at 450 °C).

Isotope data were reduced using in-house software (ArMaDiLo), at the Open University and Berkeley Geochronology Centre 'Mass Spec' software at SUERC using a decay constant value of $5.530 \times 10^{-10} \pm 0.013$ a^{-1} (Renne et al., 2011). The isotope data were corrected for blank, radioactive decay, mass discrimination and interfering reactions. The ^{40}Ar measurements from the SUERC ARGUS and OU Nu instruments were corrected for atmospheric argon via the measured ^{36}Ar. The measured ^{36}Ar on the OU MAP instrument approached detection limits, and unlike on the Nu and ARGUS, the mass discrimination is not sensitive

1C								2A				2B							
NF47		NF112		NF50		NF87		NF98		NF105		NF35		NF51		NF90		NF91	
Core	Rim	Core	Rim	Core	Rim	Core	Rim	Core	Rim	Core	Rim	Core	Rim	Core	Rim	Core	Rim	Core	Rim
36.71	36.73	36.71	36.57	36.26	36.20	37.07	37.06	35.90	36.16	34.65	34.12	36.60	36.22	36.19	36.16	36.02	38.19	36.12	35.89
2.80	2.62	2.47	2.53	2.34	2.24	1.98	1.62	2.29	2.27	2.94	2.86	2.27	2.60	2.59	2.58	2.78	2.37	2.61	2.37
16.04	16.04	17.31	16.74	16.13	16.51	17.79	18.26	17.72	17.44	15.88	16.59	16.24	16.30	15.30	15.13	16.43	16.22	15.54	15.42
0.04	0.03	0.00	0.03	0.02	0.06	0.05	0.04	0.02	0.05	0.00	0.00	0.03	0.00	0.00	0.00	0.00	0.01	0.01	0.00
18.51	18.54	16.27	15.83	17.10	17.01	16.23	16.18	18.89	18.84	20.98	20.83	19.21	19.49	19.24	18.94	22.34	20.44	22.22	22.50
0.26	0.21	0.21	0.20	0.18	0.23	0.15	0.15	0.23	0.25	0.54	0.56	0.39	0.43	0.25	0.24	0.31	0.29	0.44	0.43
11.84	11.85	12.54	12.44	12.71	12.46	11.86	11.81	10.31	10.64	8.85	8.72	10.08	9.96	11.34	11.33	7.67	6.63	7.96	8.05
0.07	0.08	0.03	0.04	0.03	0.02	0.09	0.07	0.02	0.02	0.00	0.00	0.00	0.00	0.06	0.08	0.00	2.29	0.04	0.03
0.15	0.19	0.14	0.12	0.16	0.14	0.14	0.10	0.10	0.07	0.06	0.05	0.08	0.09	0.24	0.24	0.06	0.04	0.07	0.06
9.06	9.13	9.34	9.39	9.04	9.05	9.13	9.46	9.68	9.67	9.63	9.56	9.65	9.73	9.28	9.27	9.60	8.01	9.60	9.57
0.06	0.17	0.07	0.06	0.09	0.18	0.04	0.07	0.06	0.21	0.25	0.08	0.21	0.17	0.13	0.15	0.15	0.17	0.32	0.32
0.07	0.07	0.06	0.05	0.05	0.05	0.03	0.03	0.02	0.02	0.02	0.01	0.01	0.01	0.05	0.04	0.05	0.04	0.07	0.07
95.63	95.77	95.15	94.00	94.18	94.17	94.57	94.85	95.22	95.64	93.80	93.41	94.84	95.06	94.72	94.25	95.39	94.70	95.00	94.72
Ions per 22 O																			
5.56	5.57	5.52	5.57	5.54	5.54	5.59	5.58	5.48	5.51	5.49	5.41	5.64	5.58	5.59	5.60	5.60	5.87	5.67	5.67
0.32	0.30	0.28	0.29	0.27	0.26	0.23	0.18	0.26	0.26	0.35	0.34	0.26	0.30	0.30	0.30	0.32	0.28	0.31	0.28
2.87	2.87	3.07	3.00	2.91	2.98	3.16	3.24	3.18	3.14	2.96	3.10	2.95	2.96	2.78	2.77	3.01	2.94	2.88	2.87
0.01	0.01	0.00	0.01	0.00	0.01	0.01	0.01	0.00	0.01	0.00	0.00	0.01	0.00	0.00	0.00	0.00	0.00	0.00	0.00
2.34	2.35	2.05	2.01	2.19	2.18	2.05	2.04	2.41	2.40	2.78	2.76	2.48	2.51	2.48	2.45	2.90	2.63	2.92	2.97
0.03	0.03	0.03	0.03	0.02	0.03	0.02	0.02	0.03	0.03	0.07	0.08	0.05	0.06	0.03	0.03	0.04	0.04	0.06	0.06
2.67	2.68	2.82	2.82	2.90	2.84	2.67	2.65	2.34	2.42	2.09	2.06	2.32	2.29	2.61	2.62	1.78	1.52	1.86	1.89
0.01	0.01	0.01	0.01	0.01	0.01	0.02	0.01	0.01	0.01	0.00	0.00	0.00	0.00	0.01	0.01	0.00	0.37	0.01	0.01
0.04	0.06	0.04	0.03	0.05	0.04	0.04	0.03	0.03	0.02	0.02	0.02	0.02	0.03	0.07	0.07	0.02	0.01	0.02	0.02
1.75	1.77	1.79	1.83	1.77	1.77	1.75	1.82	1.89	1.88	1.95	1.94	1.90	1.91	1.83	1.83	1.90	1.57	1.93	1.93
0.03	0.08	0.03	0.03	0.04	0.09	0.02	0.03	0.03	0.10	0.13	0.04	0.10	0.08	0.06	0.07	0.07	0.08	0.16	0.16
0.02	0.02	0.02	0.01	0.01	0.01	0.01	0.01	0.01	0.01	0.01	0.01	0.00	0.01	0.01	0.01	0.01	0.01	0.02	0.02
15.66	15.76	15.65	15.64	15.71	15.76	15.54	15.60	15.67	15.77	15.85	15.74	15.74	15.73	15.79	15.79	15.66	15.32	15.82	15.86

enough to discriminate between ^{36}Ar and ^{36}hydrocarbon. ^{40}Ar measurements from this machine were therefore only corrected for atmospheric argon when the measured ^{36}Ar was >2× that of the background measurement (c.f. Sherlock et al., 2005; Supplementary Table S.4). The dispersion in ages within and between samples vastly out-magnifies the differences in errors on the ages that these changes in correction scheme induce. Both corrected and uncorrected ages are reported in Supplementary Table S.4. Age uncertainties are reported to 2σ; uncertainties on the isotopic measurements are reported to 1σ.

4. ^{40}Ar/^{39}Ar results

The summary ^{40}Ar/^{39}Ar age data are provided in Table 3. Full isotope data for the single grain fusion analyses are reported in Supplementary Table S.4 and all ages are plotted in Fig. 3. Full UV laser ablation isotope data are in Supplementary Table S.5; ages are plotted on Fig. 4. Plots of ^{36}Ar/^{39}Ar, ^{37}Ar/^{39}Ar or ^{38}Ar/^{39}Ar vs. ^{40}Ar/^{39}Ar age show no correlation.

4.1. Single grain fusion data

4.1.1. Group 1: Garnet-bearing Gneisses

Three Group 1a samples from Krokkenakken (NF40, NF42 and NF43), totalling 34 white mica and 34 biotite analyses, yielded white mica single grain fusion (SGF) dates between 405 ± 6 Ma and 377 ± 4 Ma and biotite dates between 389 ± 2 Ma and 377 ± 2 Ma (ignoring outliers; Fig. 3A).

Six Group 1b samples, from Krokkenakken (NF106); Flatraket Harbour (NF48) and Drage (NF88, NF89, NF96 and NF99), totalling 107 white mica and 107 biotite analyses, generated white mica dates between 416 ± 8 and 373 ± 8 Ma and biotite dates between 412 ± 6 and 360 ± 6 Ma (Fig. 3B).

Four samples of white-mica-free Group 1c gneisses from Flatraket Harbour (NF47, NF112 and NF50) and Drage (NF87), yielded 63 biotite dates between 423 ± 8 and 381 ± 5 Ma (Fig. 3C).

4.1.2. Group 2: Biotite-epidote gneisses

Two samples of Group 2a gneisses from Krokkenakken (NF105) and Drage (NF98) yielded 30 white mica and 30 biotite dates between 415 ± 6 and 377 ± 9 Ma (white mica) and 393 ± 6 to 365 ± 6 Ma (biotite, Fig. 3D).

Four Group 2b samples from Krokkenakken (NF35), Flatraket Harbour (NF51) and Drage (NF90 and NF91) generated 94 biotite dates between 429 ± 4 and 377 ± 6 Ma (Fig. 3E).

4.2. UV laser ablation data

45 spots on four white mica grains from Group 1a sample NF40 and 87 spots on three white mica grains from NF43 (Fig. 4A) yielded spot dates ranging from 409 ± 3 to 380 ± 5 Ma and c. 424 ± 3 to 370 ± 6 Ma respectively (ignoring outliers, Supplementary Table S.5). Each grain provided a similar spread in dates but none showed consistent core-rim variations. 20 spots on five biotite grains from NF40 produced younger dates, from 393 ± 4 to 378 ± 3 Ma. 21 spots on five biotites from sample NF43 generated dates between 400 ± 5 and 370 ± 7 Ma.

19 spots on one large grain (~1 mm) of white mica and 18 spots on nine biotite grains from a Group 1b sample (NF48) generated dates from 390 ± 3 to 372 ± 5 Ma and 393 ± 4 to 378 ± 3 Ma respectively (ignoring outliers; Fig. 4B).

33 spots on eight grains of biotite, three included within a garnet and five within the matrix, were analysed from a sample of Group 1c gneiss (NF50) from Flatraket Harbour (Fig. 4C), producing dates between 420 ± 4 to 371 ± 4 Ma. No notable difference was determined between biotite included in garnet and those in the matrix. 24 spots on eight grains of biotite from the matrix of Group 2b sample NF51 (Fig. 4D) from Flatraket Harbour yielded dates between 433 ± 4 and 376 ± 4 Ma.

5. Diffusion modelling

The ^{40}Ar/^{39}Ar ages expected under the assumptions inherent in the Dodson T_C formulation (Dodson, 1973) for the published WGR P-T constraints were modelled using the finite-difference code DiffargP

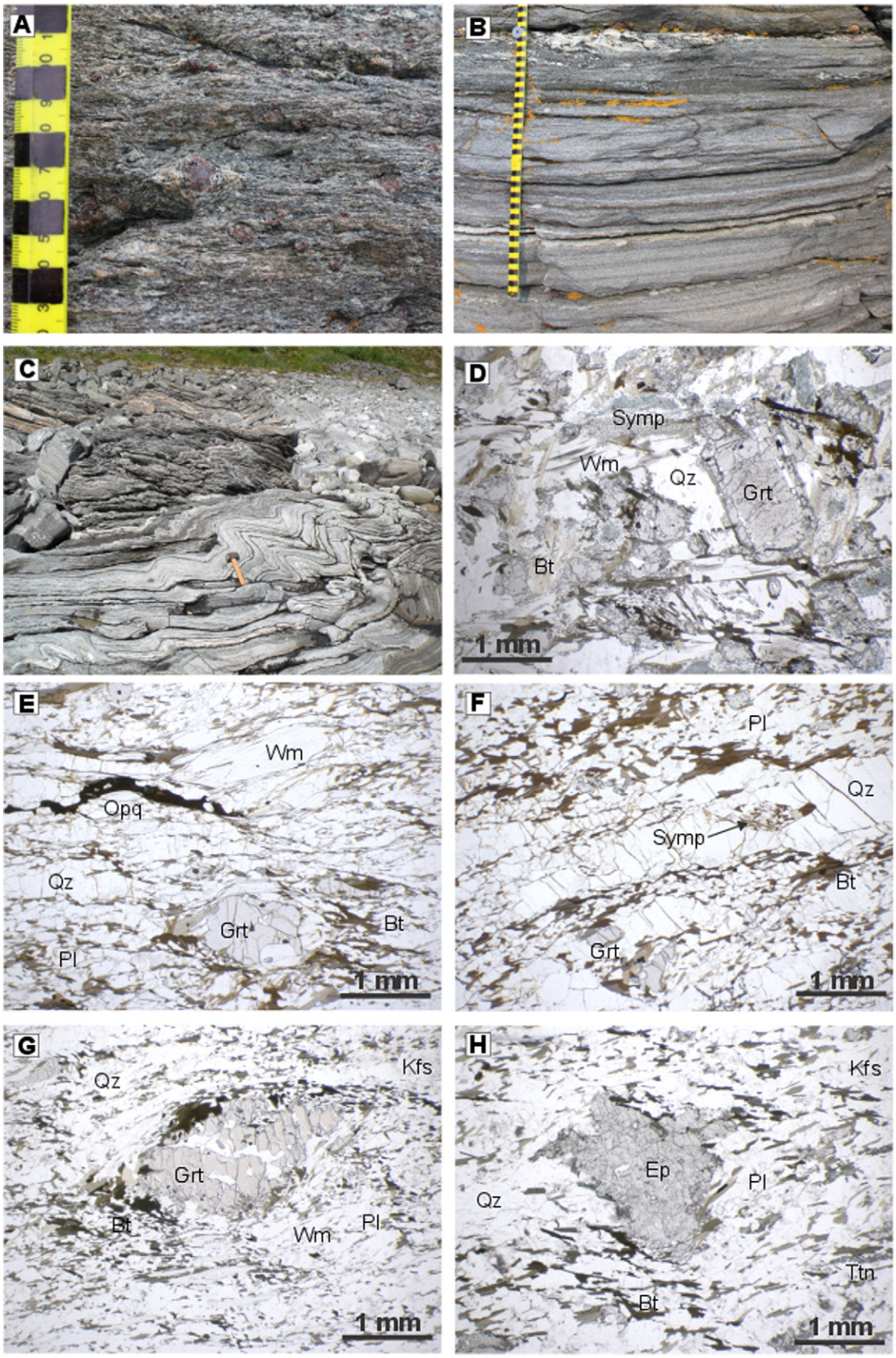

Fig. 2. Field photographs and photomicrographs of samples from the five petrological groups. (A) Field photograph of the garnet-bearing gneisses. (B) Field photograph of non-migmatised Group 2b gneiss at Flatraket Harbour. (C) Field photograph of migmatised Group 2b gneisses at Drage. (D) Group 1a gneisses (e.g. NF43) preserve high-pressure relicts. (E) Group 1b gneisses (e.g. NF48) contain relict garnet but no other HP relicts. Note the formation of white mica fish and foliation defined by biotite. (F) Group 1c gneisses (e.g. NF112) show relict symplectites of biotite + plagioclase after white mica preserved in quartz ribbons. (G) Group 2a gneisses (e.g. NF98) preserve highly degraded garnet and minor flakes of white mica and (H) Group 2b gneisses (e.g. NF51) preserve large epidote porphyroblasts but no white mica or garnet. Mineral abbreviations after Whitney & Evans (2010), Wm = white mica and Symp = symplectite.

Table 3
Summary white mica and biotite single grain fusion and in-situ ages.

				IR single grain fusion ages		UV *in-situ* ages		
				Oldest age	Youngest age		Oldest age	Youngest age
Lithology	Sample	Location	Mineral	n#	Ma (±1σ)	Ma (±1σ)	n#	Ma (±1σ)	Ma (±1σ)
Group 1a	NF40	Krokkenakken	White Mica	8	395.0 ± 2.6	387.4 ± 2.9	45	409.0 ± 2.9	380.3 ± 4.6
	NF42	Krokkenakken	White Mica	12	404.2 ± 2.6	386.7 ± 5.0		nd	nd
	NF43	Krokkenakken	White Mica	14	404.8 ± 2.7	376.8 ± 2.0	87	424.4 ± 3.0	369.8 ± 7.6
Group 1b	NF106	Krokkenakken	White Mica	15	415.6 ± 3.6	386.8 ± 4.1		nd	nd
	NF48	Flatraket Harbour	White Mica	13	391.0 ± 3.3	380.3 ± 2.9	19	389.8 ± 3.4	372.1 ± 5.4
	NF88	Drage	White Mica	25	398.84 ± 0.81	386.50 ± 0.85		nd	nd
	NF89	Drage	White Mica	24	396.5 ± 1.5	378.4 ± 4.5		nd	nd
	NF96	Drage	White Mica	15	405.5 ± 1.9	373.1 ± 3.9		nd	nd
	NF99	Drage	White Mica	15	392.3 ± 9.7	375.9 ± 3.5		nd	nd
Group 2a	NF98	Drage	White Mica	15	393.6 ± 2.2	376.7 ± 8.3		nd	nd
	NF105	Krokkenakken	White Mica	15	415.0 ± 2.4	382.4 ± 2.4		nd	nd
Group 1a	NF40	Krokkenakken	Biotite	12	437.2 ± 2.0	376.9 ± 1.0	16	393.1 ± 5.1	377.7 ± 4.0
	NF42	Krokkenakken	Biotite	10	422.3 ± 2.0	359.8 ± 1.8		nd	nd
	NF43	Krokkenakken	Biotite	12	389.4 ± 1.2	382.4 ± 1.0	21	399.6 ± 5.3	370.1 ± 8.2
Group 1b	NF106	Krokkenakken	Biotite	15	411.6 ± 3.2	396.0 ± 2.1		nd	nd
	NF48	Flatraket Harbour	Biotite	12	391.4 ± 1.2	382.4 ± 5.6	18	447.3 ± 8.8	369.8 ± 6.3
	NF88	Drage	Biotite	25	391.0 ± 0.9	378.4 ± 2.2		nd	nd
	NF89	Drage	Biotite	25	393.3 ± 0.7	377.9 ± 4.8		nd	nd
	NF96	Drage	Biotite	15	381.3 ± 1.8	359.7 ± 2.6		nd	nd
	NF99	Drage	Biotite	12	389.1 ± 3.1	375.9 ± 3.5		nd	nd
Group 1c	NF47	Flatraket Harbour	Biotite	12	414.8 ± 1.9	385.8 ± 1.8		nd	nd
	NF112	Flatraket Harbour	Biotite	15	422.8 ± 3.8	398.2 ± 2.2		nd	nd
	NF50	Flatraket Harbour	Biotite	12	400.2 ± 2.0	382.7 ± 1.0	33	419.6 ± 7.0	370.5 ± 8.6
	NF87	Drage	Biotite	25	393.1 ± 1.3	381.4 ± 4.3		nd	nd
Group 2a	NF98	Drage	Biotite	15	391.8 ± 2.0	364.8 ± 2.9		nd	nd
	NF105	Krokkenakken	Biotite	15	393.0 ± 2.9	372.3 ± 2.3		nd	nd
Group 2b	NF35	Krokkenakken	Biotite	12	428.9 ± 1.9	378.6 ± 1.0		nd	nd
	NF51	Flatraket Harbour	Biotite	25	416.0 ± 2.7	384.7 ± 1.8	24	432.8 ± 6.2	376.3 ± 3.1
	NF90	Drage	Biotite	25	398.1 ± 0.4	377.2 ± 3.2		nd	nd
	NF91	Drage	Biotite	20	390.5 ± 1.2	378.3 ± 2.8	20	nd	nd

nd = not determined n# = number of grains or spots

Krokkenakken	61°54′53.73″ N	005°20′16.49″ E
Drage	62°06′08.30″ N	005°12′48.0″ E
Flatraket Harbour	61°58′42.60″ N	005°14′03.80″ E

nd = not determined; n# = number of grains or spots

(Wheeler, 1996; Warren et al., 2012c). The P and T-dependent diffusion parameters of Harrison et al., 2009 were used to model the behaviour of white mica and the T-dependent diffusion parameters of Harrison et al., 1985 used to model the behaviour of biotite. Following petrographic observations, both micas were modelled at 0.5 mm grain radii.

Peak eclogite-facies conditions in the Nordfjord area appear to have reached 2.5–3.0 GPa and 600–700 °C at c. 410–400 Ma (U-Pb zircon), followed by isothermal decompression to 1 GPa and 700 °C by c. 399–379 Ma (U-Pb titanite: (Cuthbert et al., 2000, Root et al., 2005, Young et al., 2007, Walsh and Hacker, 2004, Spencer et al., 2013). White mica and biotite were modelled separately to reflect the fact that they experienced different post-crystallisation histories, as shown by the petrographic observations (Section 2) and as described below.

5.1. White mica models

In the Nordfjord felsic gneisses, white mica appears to be a stable member of the peak eclogite-facies assemblage. White mica models therefore assumed crystallisation under eclogite-facies conditions of 650–750 °C at 2.5–3.5 GPa. Although the white mica may have crystallised along the prograde path, previous modelling (e.g. Warren et al., 2012a) has shown that at these temperatures, Ar removal is geologically instantaneous in an open system, so regardless of when the model "clock" starts, the grain has an effective age of zero at the time cooling starts. Decompression to amphibolite-facies conditions of 700 °C at 1.0 GPa was reached 7 Ma later in the models. These constraints were based on the time difference between the youngest (400 Ma) U-Pb zircon ages assumed to constrain the timing of peak pressure metamorphism in the Nordfjord region (Root et al., 2004; Young et al., 2007), the weighted mean of the U-Pb titanite ages in the region (393 Ma; Spencer et al., 2013) and the crystallisation age of an assumed decompression-related granitic dyke (391 Ma, Kylander-Clark & Kylander-Clark and Hacker, 2014). In the models, linear cooling subsequently proceeded at a rate of 25°CMa^{-1} from amphibolite-facies conditions. This reference cooling rate is somewhat arbitrary, but uncertainties in modelled age related to the choice of cooling rate are discussed below.

5.2. Biotite models

In all the mica-bearing gneisses, biotite appears to have replaced white mica during decompression from eclogite- to amphibolite-facies conditions, and was not stable at the metamorphic peak. Biotite models therefore assumed crystallisation of ~0.5 mm radius grains at amphibolite-facies conditions of 700 °C, 1.0 GPa, followed immediately by cooling at a linear rate of 25 °C Ma^{-1}. Ar diffusion in an open system is geologically instantaneous in biotite at 700 °C, so regardless of when the biotite crystallised along the decompression path, it should only record a zero age at the time cooling initiated.

Full model results, including sensitivity testing, are presented in Table 4. The models indicate that 0.5 mm radius white mica grains that decompressed from peak eclogite-facies conditions and then cooled after reaching amphibolite-facies conditions should yield ages that are

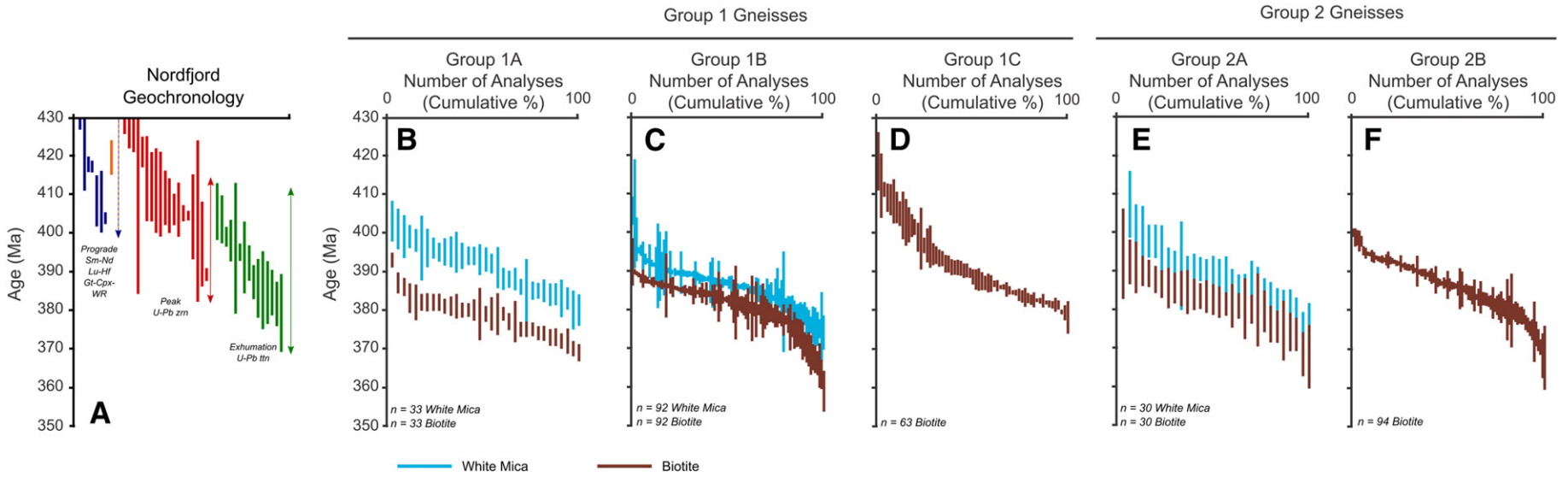

Fig. 3. (A) Compilation of current geochronological data for the Outer Nordfjord area, showing the timing of prograde metamorphism, peak metamorphism, and exhumation. Sm-Nd Grt-Cpx-Whole Rock (WR) and Lu-Hf data from Griffin and Brueckner (1980); Mearns (1986); Carswell et al., 2003; Kylander-Clark et al., 2007; and Peterman et al. (2009). U-Pb zircon data from Root et al. (2004); Young et al. (2007); Kylander-Clark and Hacker (2014); and Young and Kylander-Clark (2015). U-Pb titanite date from Spencer et al. (2013). (B–F) Cumulative graphs of white mica and biotite single-grain fusion $^{40}Ar/^{39}Ar$ data from the five petrological types.

10 Ma younger than the timing of attainment of eclogite-facies metamorphism. Similarly, 0.5 mm radius biotite grains should provide ages than are 6 Ma younger than the time at which the rocks started to cool.

The diffusion model results are sensitive to a number of input uncertainties, which can be divided into those that cause spread within the modelled ages and those that shift the whole population. The only variable that causes a spread in the resulting modelled bulk ages is grain size. Variations in grain radius between 0.25 and 1 mm produce a 1 Ma uncertainty in the modelled bulk ages, a ± 2 Ma uncertainty on the core-rim ages of white mica and ± 1 Ma uncertainty on the core-rim ages of biotite. These uncertainties are well within the 1σ error of the single grain fusion and in-situ $^{40}Ar/^{39}Ar$ ages observed in this study.

Input variables that shift the whole model population include the diffusion parameters, the modelled cooling rates, and the peak temperature. The uncertainties in the experimentally-determined diffusion parameters (E_a and D_0) shift the results by ± 4 Ma (Warren et al., 2012a). Varying the cooling rate from 10 to 50 °C Ma^{-1} causes a + 4/− 2 Ma variance in the modelled white mica age and a + 9/− 3 Ma variance in the modelled biotite age. Finally, a ± 50 °C variation in the temperature at which cooling initiates shifts the resulting model age by ± 1 Ma.

6. Discussion

6.1. New single grain fusion and in-situ data

Overall, the white mica and biotite separates from all localities and petrological groups yield a broad spread in $^{40}Ar/^{39}Ar$ ages from 416 to 373 Ma in white mica and 437–360 Ma in biotite. In-situ UV laser data

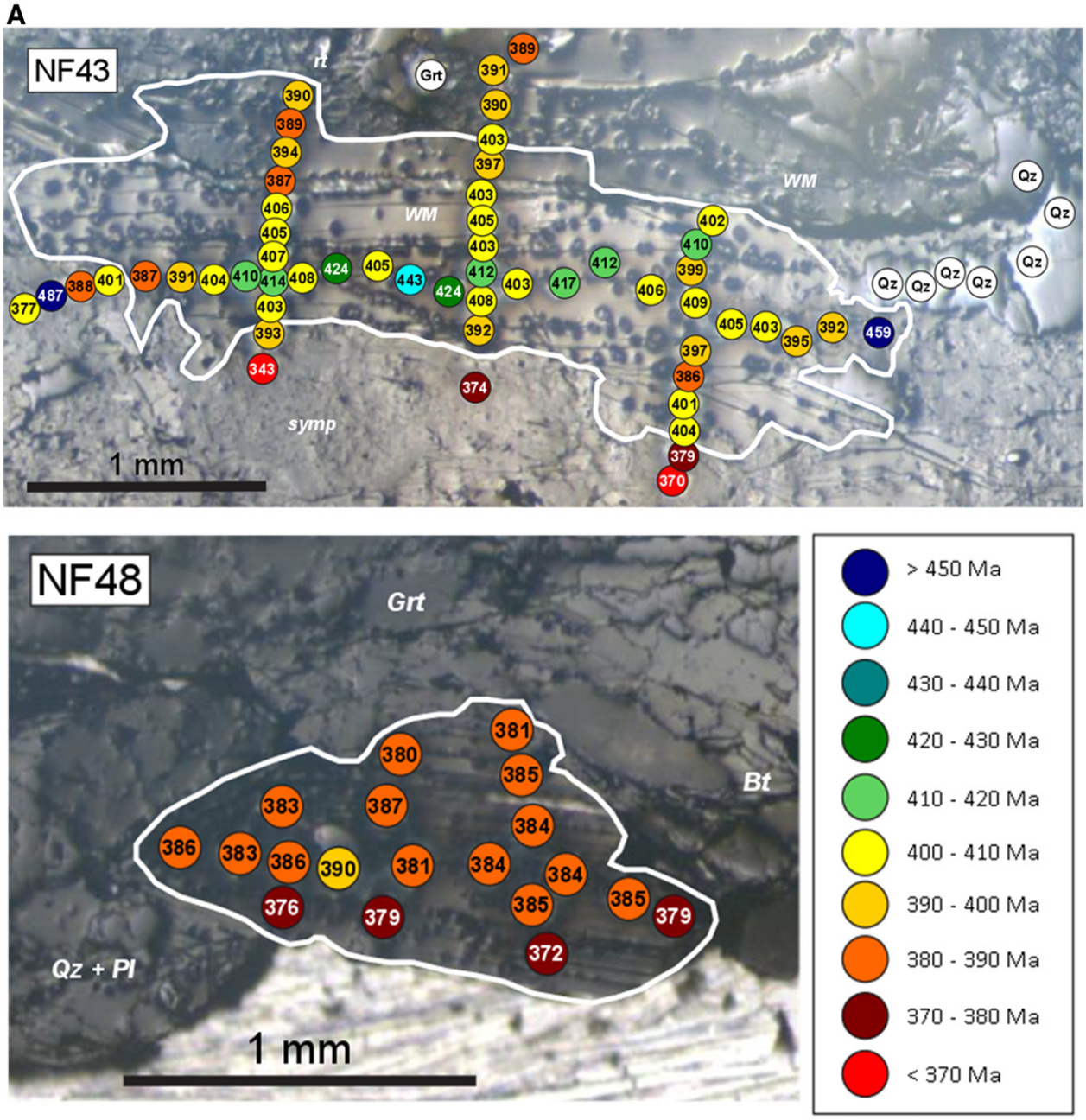

Fig. 4. A. Photomicrographs showing the in-situ UV laser ablation $^{40}Ar/^{39}Ar$ ages and analysis pits. (A) White mica in NF43 (Group 1a), (B) White mica in NF48 (Group 1b).

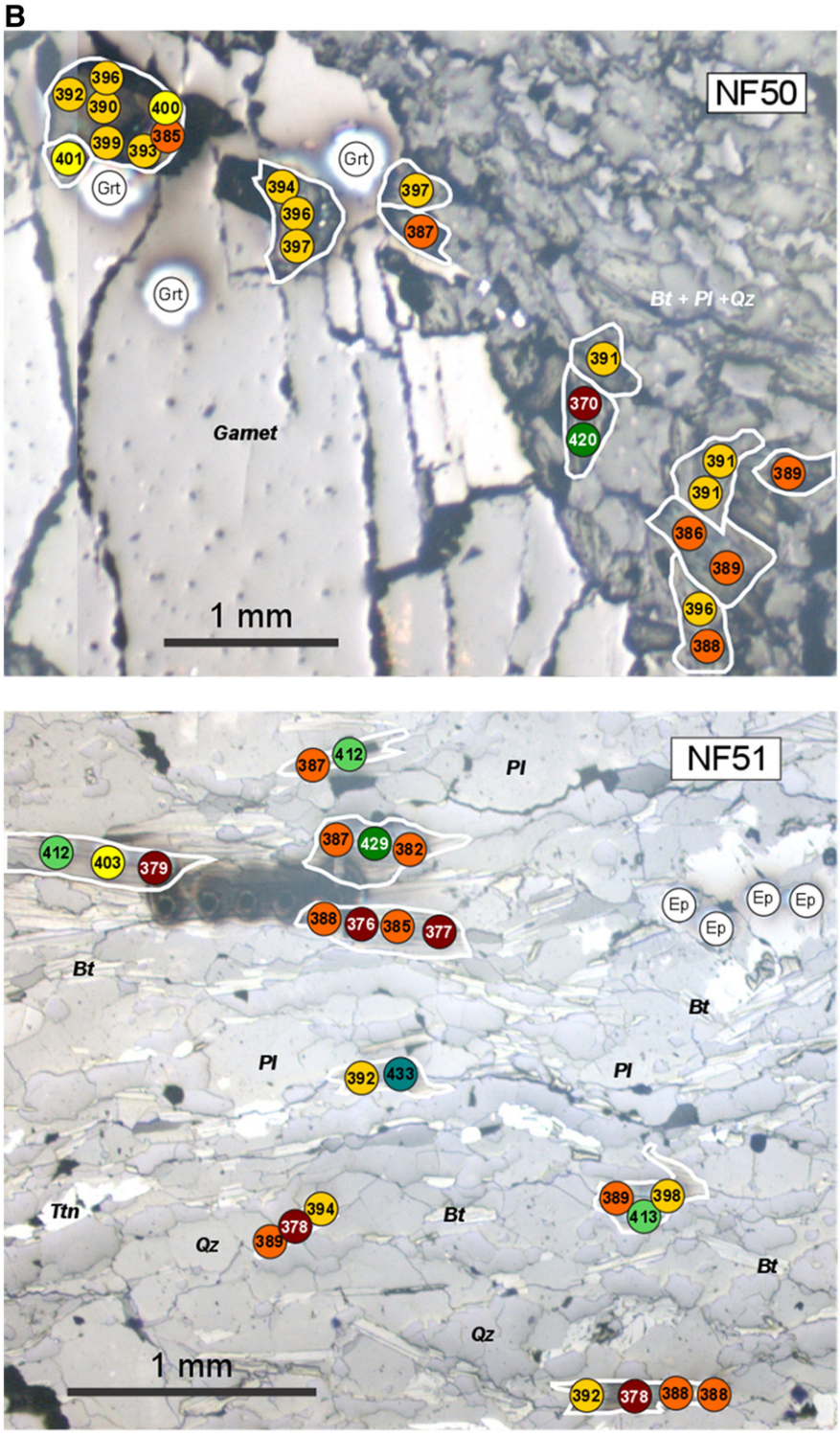

Fig. 4. B. Photomicrographs showing the in-situ UV laser ablation $^{40}Ar/^{39}Ar$ ages and analysis pits. (C) Biotite in NF50 (Group 1c), (D) Biotite in NF51 (Group 2b).

shows that the distribution of Ar both within and between grains of white mica and biotite is non-systematic and highly variable, generating ages between 424 and 370 Ma (white mica) and 440–370 Ma (biotite). Overall the in-situ analyses provided a similar, yet wider, range in the age populations compared to the single grain fusion analyses. There is no discernible difference between the ranges of ages generated from the SGF data at SUERC or the OU, despite differences in hardware.

6.2. Comparison with previously published age data

The whole $^{40}Ar/^{39}Ar$ dataset spans the known timing of the entire metamorphic cycle from prograde metamorphism at 420–404 Ma (Sm-Nd and Lu-Hf garnet; Kylander-Clark et al., 2007, Peterman et al., 2009), through peak metamorphism at c. 410–400 Ma (U-Pb zircon; Root et al., 2004; Young et al., 2007; Kylander-Clark and Hacker, 2014; Young and Kylander-Clark, 2015) to the timing of amphibolite-facies

Table 4
Diffusion modelling results.

Model	T at peak P	Peak P	Time at peak	T at amph P	P at amph	Decompression time	Post-amph cooling	Grain radius	Core age	Rim age	Bulk age	Difference from ref model
	°C	GPa	Ma	°C	GPa	Ma	°C Ma^{-1}	mm	Ma	Ma	Ma	Ma
White mica												
Reference models												
Krokkenakken	600	2.3	0	700	1.0	7	25	0.5	391	388.6	390.4	
Flatraket Harbour	700	3.0	0	700	1.0	7	25	0.5	391	388.6	390.4	
Drage	750	3.2	0	700	1.0	7	25	0.5	391	388.6	390.4	
Changes in the T at amphibolite-facies												
WM1	700	3.0	0	650	1.0	7	25	0.5	391.7	389.5	391.1	0.7
WM2	700	3.0	0	750	1.0	7	25	0.5	390.3	387.8	389.7	−0.7
Changes in P at amphibolite-facies conditions												
WM3	700	3.0	0	700	0.5	7	25	0.5	390.7	388.3	390.1	−0.3
WM4	700	3.0	0	700	1.5	7	25	0.5	391.3	389	390.7	0.3
Changes in the post-amphibolite-facies cooling rate												
WM5	700	3.0	0	700	1.0	7	10	0.5	387.2	381.6	385.8	−4.6
WM6	700	3.0	0	700	1.0	7	50	0.5	392.1	390	391.8	1.4
Changes in grain size												
WM7	700	3	0	700	1.0	7	25	1	391.5	389.1	390.8	0.4
WM8	700	3	0	700	1.0	7	25	0.25	390.5	388.1	389.9	−0.5

Model	T at amph P	P at amph	Post-amph cooling	Grain radius	Core age	Rim age	Bulk age	Difference from ref model
	°C	GPa	°C Ma^{-1}	mm	Ma	Ma	Ma	Ma
Biotite								
Reference model								
BT	700	1.0	25	0.5	395.1	395.8	387.4	
Changes in the T at amphibolite-facies								
BT1	650	1.0	25	0.5	395.9	394.8	388.3	0.9
BT2	750	1.0	25	0.5	394.2	392.8	386.5	−0.9
Changes in the post-amphibolite-facies cooling rate								
BT3	700	1.0	10	0.5	386.7	383.6	378.1	−9.3
BT4	700	1.0	50	0.5	397.7	397	390.4	3
Changes in grain size								
BT5	700	1.0	25	0.25	394.4	393.1	379.8	−7.6
BT6	700	1.0	25	1	395.7	394.5	388	0.6

recrystallization documented by U-Pb titanite at 399–379 Ma (Spencer et al., 2013).

Published white mica $^{40}Ar/^{39}Ar$ step heating plateau ages for the Outer Nordfjord area, range from *c.* 409–380 Ma (Root et al., 2005; Young et al., 2011). White mica SGF and in-situ $^{40}Ar/^{39}Ar$ ages from this study span a greater range from 416 to 373 Ma and 424–370 Ma, respectively. The ages generated in this study are also broadly similar to previously reported SGF and in-situ ages for felsic gneisses and garnet mica schists from the Outer Nordfjord area (413 ± 4 Ma to 379 ± 2 Ma and 507 ± 6 Ma to 388 ± 6 Ma, respectively; Warren et al., 2012a).

Published biotite $^{40}Ar/^{39}Ar$ step heating plateau ages from the WGR, range from 467 to 379 Ma (Berry et al., 1995; Hacker and Gans, 2005; Root et al., 2005). Biotite SGF and in-situ ages from this study range from 437 to 360 Ma and 447–370 Ma, respectively, within the previously reported range.

Previous studies have interpreted white mica and biotite step heating ages from Western Norway as representing the timing of cooling through 400 °C and 350 °C, respectively (Root et al., 2005; Hacker, 2007; Walsh et al., 2007; Young et al., 2011; Walsh et al., 2013). However, the age ranges documented in this study both within and between grains, and within and between samples, suggest there may be a more complex link between $^{40}Ar/^{39}Ar$ age and metamorphic evolution. The different lithologies studied here allow the ages to be considered in relation to different potential influences.

6.3. Ar (re)distribution during a metamorphic cycle

There are several possible explanations for the broad range of $^{40}Ar/^{39}Ar$ dates - spanning 45/47 Ma (SGF/in-situ) in white mica and 77/70 Ma in biotite. These include the loss or gain of Ar due to diffusion, recrystallization, deformation, partial melting and/or the availability and/or influence of fluids. The effect of each of these processes can be critically assessed by comparing and contrasting age populations of different samples.

6.3.1. Diffusion

The diffusion models show that in open conditions at temperatures of ~700 °C, volume diffusion in white mica and biotite should have been sufficient to reset mica ages in the Nordfjord area prior to the initiation of cooling. White mica grains of 0.5 mm diameter that crystallised at eclogite facies conditions should provide ages that are ~10 Ma younger than their crystallisation age. Similarly, 0.5 mm biotite grains that crystallised under amphibolite facies conditions should yield ages than are ~6 Ma younger their crystallisation age, assuming cooling started soon after they crystallised. White mica grains from the study area should therefore produce total fusion ages of ~390 Ma with core-rim ages that range from 391 to 389 Ma. Biotite should provide bulk (total fusion) ages of ~387 Ma and core-rim ages that range from 388 to 387 Ma. However only ~20% of the white mica and biotite single grain fusion ages lie within the suggested model ages ±2 Ma (Fig. 3). 50% of the white mica SGF ages and 65% of the white mica in-situ ages, and 48% of the biotite SGF ages and 59% of the biotite in-situ ages are older, suggesting that diffusion may not be the principle mechanism for Ar redistribution within and between the micas of these felsic gneisses.

A key prediction of the pure diffusion model is the development of systematic core-rim age variations: older cores and younger rims. The in-situ white mica $^{40}Ar/^{39}Ar$ data show patchy age distributions, with the oldest ages not necessarily concentrated in geographic grain cores and no clear core-rim age profiles (Fig. 4a). Biotite yields a relatively more homogeneous spread of in-situ ages, with little variation in age between single grains in different petrographic contexts, despite the variations in composition and metamorphic grade (Fig. 4b). Given the

analytical uncertainties for the biotite in-situ data (around ±6 Ma), the ±1 Ma core-rim age variation suggested by the diffusion modelling is not resolvable.

Together, the spread in SGF and in-situ ages within and between both grains in the same sample and across different samples suggests that diffusion was not the sole mechanism by which Ar was redistributed within both white mica and biotite, despite cooling from ambient temperatures of ~700 °C.

6.3.2. White Mica breakdown

Mica recrystallization during metamorphism may exert a far greater influence on isotopic resetting than diffusion, and should outpace it (e.g. Villa, 1998; Allaz et al., 2011). In our samples, the white mica appears to have been the only stable K-bearing phase at peak eclogite-facies conditions. As exhumation and decompression progressed, white mica recrystallized to biotite + plagioclase. Various samples of Group 1 gneiss document differential progress of this reaction, culminating in some samples in the complete loss of white mica (NF43, NF48, and NF50; Fig. 5A and B). White mica and biotite age populations in these samples were compared using Student T Tests to evaluate whether any statistically different significance were exhibited. The results are presented in Table 5.

Sample NF43 (Group 1a) preserves the initial stages of white mica breakdown to biotite. In this sample, white mica SGF ages range from 404 to 387 Ma and biotite SGF ages from 390 to 383 Ma (Table 3, Fig. 5A and B). Sample NF48 preserves more advanced breakdown of white mica and yields a statistically younger white mica age population of 391–380 Ma. The biotite age population in sample NF48, however, is statistically identical to sample NF43 (391–382 Ma; Fig. 5A and B). This suggests that even though ^{40}Ar was being released during white mica breakdown, it was not incorporated into the concurrently crystallising biotite in either sample. Conversely, biotite in sample NF50, which preserves no white mica, generated statistically significantly older ages of 400–383 Ma (Fig. 5B). This shift towards older dates implies that the co-crystallising biotite incorporated some of the ^{40}Ar released from the white mica, assuming all the biotite crystallised during exhumation. A recent study suggests that in some samples, lower pressure minerals persisted metastably during the Caledonian orogeny (Young and Kylander-Clark, 2015). If this was the case for biotite, some of the older ages may imply argon inheritance. Either way, the data suggest that an open system was not consistently or concurrently present in all rock types during exhumation.

6.3.3. Deformation

The effect of exhumation-related deformation on the ^{40}Ar/^{39}Ar ages yielded by the felsic lithologies was investigated by comparing the white mica and biotite SGF ages from Group 1a and Group 1b gneisses, which are assumed to be of the same bulk composition (Fig. 5C and D). Group 1a gneisses preserve biotite-plagioclase symplectites that form from the breakdown of white micas. These delicate structures suggest that little or no deformation affected these gneisses during and/or after decompression (e.g. Hacker et al., 2010). These samples also variably preserve HP relicts such as omphacite or kyanite that are not present in the other gneiss groups. In contrast, Group 1b gneisses do not preserve the delicate symplectite structure, but are instead deformed, with a gneissic foliation defined by biotite + plagioclase. White micas are kinked, folded and form "fish" and HP minerals or their relicts are not present. The Si content of the remnant white mica in Group 1b is more variable than that in Group 1a.

White mica and biotite in Group 1a samples yielded SGF ages between 405 and 377 Ma and 437–360 Ma, respectively (Table 3). Group 1b samples generated broader, but statistically identical age ranges (416–373 Ma and 412–360 Ma; Tables 3 and 5). The age population similarity between the two groups suggests that in this area, formation of the gneissic fabric does not result in a statistically significant change in the white mica and biotite ^{40}Ar/^{39}Ar age populations.

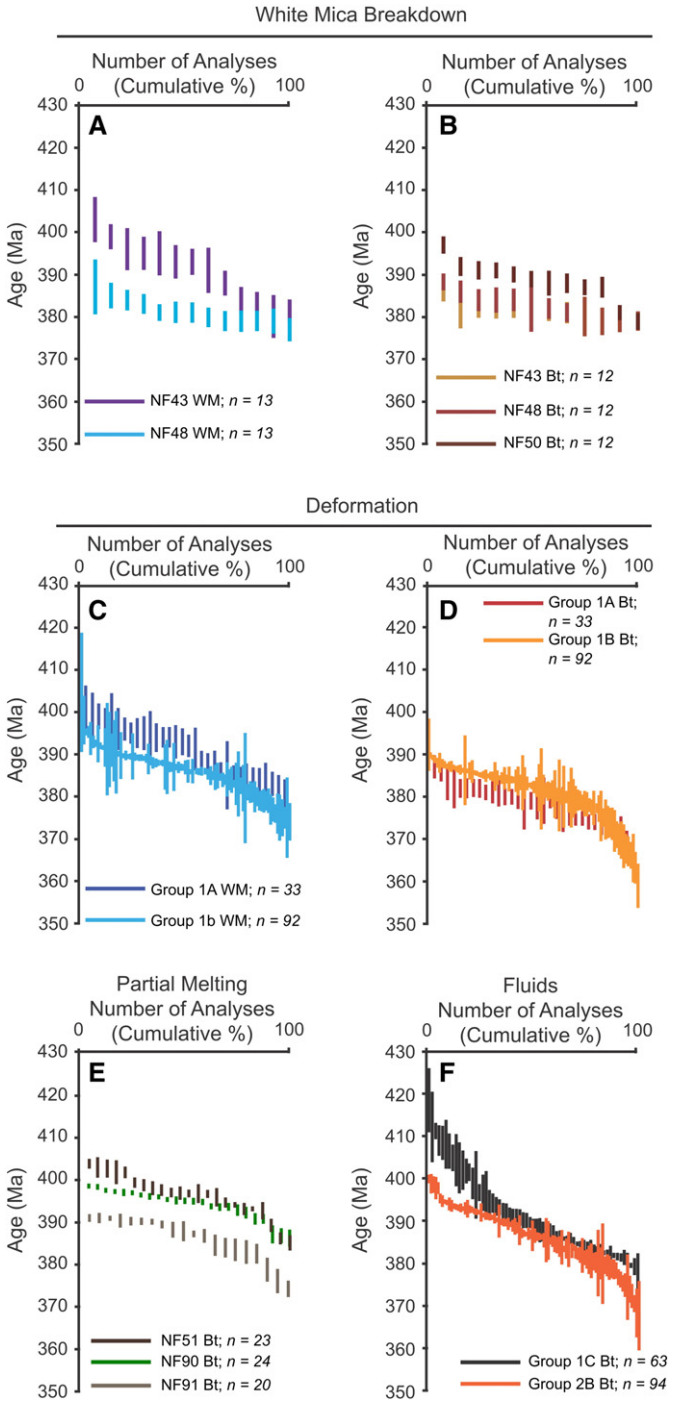

Fig. 5. Cumulative graphs of single-grain fusion data showing the effect on the ^{40}Ar/^{39}Ar ages of different processes. WM = white mica; Bt = biotite. (A & B) Progressive white mica replacement by biotite + plagioclase in samples NF43, NF48, and NF50. (C & D) The effect of deformation between two type of garnet-bearing gneisses from Group 1a and Group 1B. (E) The effect of partial melting on samples NF51, NF90, and NF91. (F) The effect of fluid infiltration between samples from Group 1c and Group 2b gneisses.

Assuming the fabric is related to Caledonian deformation, rather than inherited from the Proterozoic protolith (e.g. Young and Kylander-Clark, 2015); the implication is that deformation alone did not control ^{40}Ar redistribution in the felsic gneisses.

6.3.4. Partial melting

Migmatites have been documented in many exhumed HP metamorphic complexes (e.g. Faure et al., 1999; Hermann et al., 2001; Ganzhorn

Table 5
Student *t*-test results.

White Mica

All Data	Group 1a	Group 1b
Group 1a		
Group 1b	0.09	
Group 2a	**0.26**	**0.87**

Recrystallisation	NF43 WM
NF43 WM	
NF48 WM	0.00

Deformation	Group 1a WM
Group 1a WM	
Group 1b WM	0.09

Values < **0.05** indicate significant difference at 95% confidence
Values **0.05–0.1** indicate a possible difference at 95% confidence
Values > **0.1** indicate no significant difference at 95% confidence

(WM = white mica, Bt = biotite)

Biotite

All Data	Group 1a	Group 1b	Group 1c	Group 2a
Group 1a				
Group 1b	0.06			
Group 1c	0.00	0.00		
Group 2a	**0.31**	**0.23**	0.00	
Group 2b	0.00	0.00	0.04	0.00

Recrystallisation	NF43 Bt	NF48 Bt
NF43 Bt		
NF48 Bt	**0.30**	
NF50 Bt	0.00	0.00

Deformation	Group 1a Bt
Group 1a Bt	
Group 1b Bt	0.06

Fluids	Group 1c Bt
Group 1c Bt	
Group 2b Bt	0.04

Partial Melting	NF51 Bt
NF51 Bt	
NF91 Bt	0.00

Partial Melting	NF90 Bt	NF91 Bt	NF51 Bt
NF90 Bt			
NF91 Bt	0.00		
NF51 Bt	0.09	0.00	

et al., 2014), with melting generally linked to decompression from eclogite- to the amphibolite-facies conditions at high temperatures (e.g. Labrousse et al., 2002). At Drage, the amphibolite-facies gneisses show abundant field and petrological evidence for partial melting (Fig. 2C, Supplementary information S2). The $^{40}Ar/^{39}Ar$ ages of key Group 2b gneisses (samples NF90 and NF91 from Drage, and NF51 from Flatraket Harbour) were compared to assess the influence of partial melting on the $^{40}Ar/^{39}Ar$ signature. NF90 and NF91 were collected within 40 cm of each other; the former is a non-migmatised augen gneiss, whilst the latter shows extensive migmatisation. Sample NF51 has the same mineral assemblage as sample NF91, but shows no field or petrological evidence for melting (Fig. 2B, Supplementary information S2).

Biotite in the migmatitic sample NF91 yielded $^{40}Ar/^{39}Ar$ ages of 391–378 Ma, whereas biotite in non-migmatised samples NF51 and NF90 generated statistically significantly older populations of 416–385 Ma and 398–386 Ma, respectively (Fig. 5E). Partial melting in these samples may have therefore caused the younging in the $^{40}Ar/^{39}Ar$ age populations, possibly by increasing the interconnectivity of the grain boundary network, and hence aiding the local removal of Ar from the system. This effect is apparent even on a local-scale, given the close proximity of samples NF90 and NF91. Further studies involving a greater number of melted vs. non-melted samples are needed to test this finding further, as there may be other confounding factors.

6.3.5. Fluids

Fluids may control resetting of $^{40}Ar/^{39}Ar$ mineral ages in metamorphic rocks by enhancing transport pathways and assisting recrystallization reactions (e.g. Cumbest et al., 1994; Kelley, 2002). Fluids can be derived from local dehydration reactions during retrogression (e.g. white mica breaks down to produce biotite + plagioclase + fluid), or be derived from external sources such as surrounding rocks.

The felsic rocks exposed in the Outer Nordfjord region preserve evidence for fluid-producing reactions during their decompression history, including the white mica breakdown reaction. In contrast, the replacement of garnet (Group 1c gneisses) by epidote–group minerals (Group 2b gneisses) consumed fluids. Together these reactions show that water was both locally produced and consumed in the felsic rocks during exhumation, and that fluid was likely mobile at least on the cm scale.

The influence of fluid availability on the biotite $^{40}Ar/^{39}Ar$ ages between the garnet- and epidote-bearing samples is clear (Fig. 5F). The garnet-bearing rocks of Group 1c yielded biotite ages of 423–381 Ma, whereas the epidote-bearing rocks of Group 2b generated a statistically older and broader population between 429 and 377 Ma. Fluid in the Group 2b gneisses, likely internally-derived from the white mica breakdown reaction, therefore appears to not have been very mobile. The older biotite population and the increased age spread suggest that the grain boundary network was (partially) closed during exhumation. Fluid may have become highly enriched in ^{40}Ar during the mica breakdown reaction, resulting in a source rather than a sink for ^{40}Ar during biotite crystallisation.

6.3.6. Summary

The lack of clear core-rim age variations expected from diffusive loss and the wide spread in ages shown by the SGF data suggest that diffusion was not the primary mechanism by which ^{40}Ar was redistributed in micas from the WGR felsic gneisses. Furthermore, the lack of statistical difference between age populations in samples that record strain during the Caledonian orogeny vs. those that do not suggests that in this region at least, deformation was unimportant for redistributing Ar. Conversely, white mica breakdown, partial melting and the release/absorption of fluids appear to have played a far greater role in controlling grain ^{40}Ar concentrations.

Samples in which white mica is no longer present (but for which textural evidence of precursor white mica is still visible) yield older biotite age populations than samples in which white mica is still present. Rocks in which there is evidence for partial melting produce younger biotite age populations than rocks which do not appear to have melted, suggesting that melting facilitated ^{40}Ar removal. The older biotite age population in more hydrated samples compared to drier samples suggests that fluid released during white mica breakdown acted as a source for 'excess' ^{40}Ar in the biotite and that the fluid had limited mobility.

7. Conclusions

Felsic gneisses with similar bulk compositions from the Outer Nordfjord area of the UHP Western Gneiss Region, Norway, preserve textural and petrological evidence of different stages of their burial and exhumation history. $^{40}Ar/^{39}Ar$ data show that Ar is incorporated into, hosted by, and ultimately lost by white mica and biotite differently in these different rock types despite their shared metamorphic history.

White mica and biotite grains yield dispersed single grain fusion age populations from 416 to 373 Ma and 437 to 360 Ma, respectively. In-situ UV laser ablation white mica analyses reveal a similar, but older, 424 to 370 Ma spread within individual grains, and no clear core-rim patterns. In-situ biotite analyses yield a similar, and slightly older, spread, from 447 to 370 Ma.

Numerical modelling of open system diffusion predicts that due to the high temperatures experienced by the WGR during the metamorphic cycle, white mica and biotite ages should reflect the timing of cooling after reaching amphibolite-facies conditions. However both micas yield age populations that are mostly older than the model ages and span the timing of the entire metamorphic cycle. Such an age spread cannot be reconciled with simple open system diffusion and therefore the Outer Nordfjord $^{40}Ar/^{39}Ar$ mica ages likely do not strictly represent the timing of cooling through a discrete temperature or temperature interval. Whilst Ar must have diffused readily within minerals during the exhumation of the WGR at temperatures near 700 °C, age populations in samples that record different parts of the metamorphic cycle suggest that processes such mineral breakdown, partial melting, and fluid availability had a greater effect on Ar redistribution and eventual $^{40}Ar/^{39}Ar$ age at the grain- to outcrop-scale. In detail, samples recording significant white mica breakdown produced younger white mica dates than white mica in less retrogressed samples. These ages were overall too old to be interpreted as crystallisation or cooling ages. In the same sample suite, biotite grains yielded the same age population in samples that still contained white mica or white mica remnants, but an older population in the samples where white mica had completely broken down. Samples that showed significant evidence for partial melting generated a younger biotite population than samples showing no evidence for partial melting. More hydrated (epidote-present) samples provided significantly older biotite age populations than less hydrated (garnet-present) samples. The older biotite population in the more hydrated samples suggests high ^{40}Ar concentrations were present in the fluids and that local fluid mobility was limited. Finally, contrary to previous studies, deformation did not appear to affect the $^{40}Ar/^{39}Ar$ mica age populations in these samples.

The spread of ages generated both within and between different samples has repercussions for detrital mica provenance studies. These studies assume that the source material can be defined by specific $^{40}Ar/^{39}Ar$ age populations that reflect the cooling and exhumation history of the source. In the WGR, this source material is predominately felsic gneiss, which, in this study, yield spreads of up to 46 Ma (white mica) and 74 Ma (biotite) from the same exposure horizon. Matching detrital mica populations to a change in source in this region is therefore impossible.

This study shows that the interpretation of $^{40}Ar/^{39}Ar$ age data collected from high temperature metamorphic terranes is assisted by analysing different Ar chronometers and multiple samples that record different parts of the metamorphic cycle. Data from different rock types needs to be considered on a case-by-case basis, in conjunction with detailed petrographic analysis, before $^{40}Ar/^{39}Ar$ mica ages can be interpreted.

Supplementary data to this article can be found online at http://dx.doi.org/10.1016/j.chemgeo.2016.09.028.

Acknowledgements

CSM was funded on an Open University Charter Studentship. CJW acknowledges financial support from a NERC Advanced Fellowship (NE/H016279/1). Laboratory and technical assistance from Michelle Higgins, Sam Hammond and James Malley was gratefully received. David Young, Jan. Wijbrans and Klaus Mezger are all thanked for insightful comments that improved the manuscript.

References

Allaz, J., Engi, M., Berger, A., Villa, I.M., 2011. The effects of retrograde reactions and of diffusion on $^{40}Ar/^{39}Ar$ ages of micas. J. Petrol. 52, 691–716. http://dx.doi.org/10.1093/petrology/egq100.

Arnaud, N., Kelley, S., 1995. Evidence for excess argon during high pressure metamorphism in the Dora Maira massif (western Alps, Italy), using an ultra-violet laser ablation microprobe $^{40}Ar/^{39}Ar$ technique. Contrib. Mineral. Petrol. 121, 1–11. http://dx.doi.org/10.1007/s004100050086.

Baxter, E.F., DePaolo, D.J., Renne, P.R., 2002. Spatially correlated anomalous $^{40}Ar/^{39}Ar$ "age" variations in biotites about a lithologic contact near Simplon Pass, Switzerland: a mechanistic explanation for excess Ar. Geochim. Cosmochim. Acta 66, 1067–1073. http://dx.doi.org/10.1016/S0016-7037(01)00828-6.

Berry, H.N., Lux, D.R., Andresen, A., Andersen, T.B., 1995. Progressive exhumation during orogenic collapse as indicated by $^{40}Ar/^{39}Ar$ cooling ages from different structural levels, southwest Norway. Geolognytt 22, 20–21.

Bryhni, I., 1966. Reconnaissance studies of gneisses, ultrabasites, eclogites and anorthosites in outer Nordfjord, western Norway. Norges Geologiske Undersokelse 241, 1–68.

Carswell, D.A., Brueckner, H.K., Cuthbert, S.J., Metha, K., O'Brien, P.J., 2003. The timing of stabilisation and the exhumation rate for the ultra-high pressure rocks in the Western Gneiss Region of Norway. J. Metamorph. Geol. 21, 601–612. http://dx.doi.org/10.1046/j.1525-1314.2003.00467.x.

Cumbest, R.J., Johnson, E.L., Onstott, T.C., 1994. Argon composition of metamorphic fluids: Implications for $^{40}Ar/^{39}Ar$ geochronology. Geol. Soc. Am. Bull. 106, 942–951. http://dx.doi.org/10.1130/0016-7606(1994)106<0942:ACOMFI>2.3.CO.

Cuthbert, S.J., Carswell, D.A., Krogh-Ravna, E.J., Wain, A., 2000. Eclogites and eclogites in the Western Gneiss Region, Norwegian Caledonides. Lithos 52, 165–195. http://dx.doi.org/10.1016/S0024-4937(99)00090-0.

Di Vincenzo, G., 2004. The relationship between tectono-metamorphic evolution and argon isotope records in white mica: constraints from in situ ^{40}Ar-^{39}Ar laser analysis of the Variscan basement of Sardinia. J. Petrol. 45, 1013–1043. http://dx.doi.org/10.1093/petrology/egh002.

Dodson, M.H., 1973. Closure temperature in cooling geochronological and petrological systems. Contrib. Mineral. Petrol. 40, 259–274.

Eskola, P., 1921. On the eclogites of Norway. Norske vidsenskaps-akademi i Oslo. Matematisk-naturvidenskabelig klasse 8, 1–118.

Faure, M., Lin, W., Shu, L., Sun, Y., Schärer, U., 1999. Tectonics of the Dabieshan (eastern China) and possible exhumation mechanism of ultra-high-pressure rocks. Terra Nova 11, 251–258. http://dx.doi.org/10.1046/j.1365-3121.1999.00257.x.

Foland, K., 1979. Limited mobility of argon in a metamorphic terrane. Geochim. Cosmochim. Acta 43, 793–801. http://dx.doi.org/10.1016/0016-7037(79)90219-9.

Ganzhorn, A.C., Labrousse, L., Prouteau, G., Leroy, C., Vrijmoed, J.C., Andersen, T.B., Arbaret, L., 2014. Structural, petrological and chemical analysis of syn-kinematic migmatites: Insights from the western gneiss region, Norway. J. Metamorph. Geol. 647–673 http://dx.doi.org/10.1111/jmg.12084.

Gee, D.G., 1975. A tectonic model for the central part of the Scandinavian Caledonides. Am. J. Sci. 275-A, 468–515.

Griffin, W.L., Brueckner, H.K., 1980. Caledonian Sm-Nd ages and a crustal origin for Norwegian eclogites. Nature 285, 319–321. http://dx.doi.org/10.1038/285319a0.

Hacker, B.R., 2007. Ascent of the ultrahigh-pressure Western Gneiss Region, Norway. Geol. Soc. Am. Spec. Paper 419, 171–184. http://dx.doi.org/10.1130/2006.2419(09.

Hacker, B.R., Gans, P.B., 2005. Continental collisions and the creation of ultrahigh-pressure terranes: petrology and thermochronology of nappes in the central Scandinavian Caledonides. Geol. Soc. Am. Bull. 117, 117–134. http://dx.doi.org/10.1130/B25549.1.

Hacker, B.R., Andersen, T.B., Johnson, S., Kylander-Clark, A.R.C., Peterman, E.M., Walsh, E.O., Young, D.J., 2010. High-temperature deformation during continental-margin subduction & exhumation: the ultrahigh-pressure Western Gneiss Region of Norway. Tectonophysics 480, 149–171. http://dx.doi.org/10.1016/j.tecto.2009.08.012.

Harrison, T.M., Duncan, I., McDougall, I., 1985. Diffusion of ^{40}Ar in biotite: temperature, pressure and compositional effects. Geochim. Cosmochim. Acta 49, 2461–2468. http://dx.doi.org/10.1016/0016-7037(85)90246-7.

Harrison, T.M., Célérier, J., Aikman, A.B., Hermann, J., Heizler, M.T., 2009. Diffusion of ^{40}Ar in muscovite. Geochim. Cosmochim. Acta 73, 1039–1051. http://dx.doi.org/10.1016/j.gca.2008.09.038.

Hermann, J., Rubatto, D., Korsakov, A., Shatsky, V.S., 2001. Multiple zircon growth during fast exhumation of diamondiferous, deeply subducted continental crust (Kokchetav

Massif, Kazakhstan). Contrib. Mineral. Petrol. 141, 66–82. http://dx.doi.org/10.1007/s004100000218.
Kelley, S.P., 2002. Excess argon in K–Ar and Ar–Ar geochronology. Chem. Geol. 188, 1–22. http://dx.doi.org/10.1016/S0009-2541(02)00064-5.
Krabbendam, M., Wain, A., 1997. Late-Caledonian structures, differential retrogression and structural position of (ultra)high-pressure rocks in the Nordfjord-Stadlandet area, Western Gneiss Region. Norges Geologiske Undersokelse Bulletin 432, 127–139.
Kylander-Clark, A.R.C., Hacker, B.R., 2014. Age and significance of felsic dykes from the UHP Western Gneiss Region. Tectonics 33, 2342–2360. http://dx.doi.org/10.1002/2014TC003582.
Kylander-Clark, A.R.C., Hacker, B.R., Johnson, C., Beard, B., Mahlen, N., Lapen, T., 2007. Coupled Lu–Hf and Sm–Nd geochronology constrains prograde and exhumation histories of high- and ultrahigh-pressure eclogites from western Norway. Chem. Geol. 242, 137–154. http://dx.doi.org/10.1016/j.chemgeo.2007.03.006.
Labrousse, L., Jolivet, L., Agard, P., Hébert, R., Andersen, T., 2002. Crustal-scale boudinage and migmatization of gneiss during their exhumation in the UHP Province of Western Norway. Terra Nova 14, 263–270. http://dx.doi.org/10.1046/j.1365-3121.2002.00422.x.
Labrousse, L., Jolivet, L., Andersen, T.B., Agard, P., Hérbert, R., Maluski, H., Schärer, U., 2004. Pressure-temperature-time deformation history of the exhumation of ultra-high pressure rocks in the Western Gneiss Region, Norway. In: Whitney, D.L., Teyssier, C., Siddoway, C.S. (Eds.), Gneiss Domes in Orogeny 380. Geological Society of America Special Paper, pp. 155–183.
Li, S., Wang, S., Chen, Y., Liu, D., Qiu, J., Zhou, H., Zhang, Z., 1994. Excess argon in phengite from eclogite: evidence from dating of eclogite minerals by Sm/Nd, Rb/Sr and $^{40}Ar/^{39}Ar$ methods. Chem. Geol. 112, 343–350. http://dx.doi.org/10.1016/0009-2541(94)90033-7.
Lux, D.R., 1985. K/Ar ages from the Basel Gneiss Region, Stadlandet area, Western Norway. Nor. Geol. Tidsskr. 65, 277–286.
Mark, D.F., Barfod, D., Stuart, F.M., Imlach, J., 2009. The ARGUS multicollector noble gas mass spectrometer: performance for $^{40}Ar/^{39}Ar$ geochronology. Geochem. Geophys. Geosyst. 10, Q0AA02. http://dx.doi.org/10.1029/2009GC002643.
Mark, D.F., Rice, C.M., Fallick, A.E., Trewin, N.H., Lee, M.R., Boyce, A., Lee, J.K.W., 2011. $^{40}Ar/^{39}Ar$ dating of hydrothermal activity, biota and gold mineralization in the Rhynie hot-spring system, Aberdeenshire, Scotland. Geochim. Cosmochim. Acta 75, 555–569. http://dx.doi.org/10.1016/j.gca.2010.10.014.
Mearns, E.W., 1986. Sm-Nd ages for Norwegian garnet peridotite. Lithos 19, 269–278. http://dx.doi.org/10.1016/0024-4937(86)90027-7.
Peterman, E.M., Hacker, B.R., Baxter, E.F., 2009. Phase transformations of continental crust during subduction and exhumation: Western Gneiss Region, Norway. Eur. J. Mineral. 21, 1097–1118. http://dx.doi.org/10.1127/0935-1221/2009/0021-1988.
Pickles, C.S., Kelley, S.P., Reddy, S.M., Wheeler, J., 1997. Determination of high spatial resolution argon isotope variations in metamorphic biotites. Geochim. Cosmochim. Acta 61, 3809–3833. http://dx.doi.org/10.1016/S0016-7037(97)00289-5.
Renne, P.R., Balco, G., Ludwig, K.R., Mundil, R., Min, K., 2011. Response to the comment by Schwarz et al., on joint determination of ^{40}K decay constants and $^{40}Ar^*/^{40}K$ for the Fish Canyon sanidine standard, and improved accuracy for $^{40}Ar/^{39}Ar$ geochronology by P.R. Renne et al. (2010). Geochim. Cosmochim. Acta 75, 5097–5100. http://dx.doi.org/10.1016/j.gca.2011.06.021.
Roberts, D., 2003. The Scandinavian Caledonides: event chronology, palaeogeographic settings and likely modern analogues. Tectonophysics 365, 283–299. http://dx.doi.org/10.1016/S0040-1951(03)00026-X.
Root, D.B., Hacker, B.R., Mattinson, J.M., Wooden, J.L., 2004. Zircon geochronology and ca. 400 Ma exhumation of Norwegian ultrahigh-pressure rocks: an ion microprobe and chemical abrasion study. Earth Planet. Sci. Lett. 228, 325–341. http://dx.doi.org/10.1016/j.epsl.2004.10.019.
Root, D.B., Hacker, B.R., Gans, P.B., Ducea, M.N., Eide, E.A., Mosenfelder, J.L., 2005. Discrete ultrahigh-pressure domains in the Western Gneiss Region, Norway: implications for formation and exhumation. J. Metamorph. Geol. 23, 45–61. http://dx.doi.org/10.1111/j.1525-1314.2005.00561.x.
Ruffet, G., Gruau, M., Ballevre, M., Feraud, G., Philippot, P., 1997. Rb/Sr and $^{40}Ar/^{39}Ar$ laser probe dating of high-pressure phengites from the Sesia zone (Western Alps): underscoring of excess argon and new age constraints on the high-pressure metamorphism. Chem. Geol. 141, 1–18. http://dx.doi.org/10.1016/S0009-2541(97)00052-1.
Scaillet, S., 1996. Excess ^{40}Ar transport scale and mechanism in high-pressure phengites: a case study from an eclogitized metabasites of the Dora-Maira nappe, western Alps. Geochim. Cosmochim. Acta 60, 1075–1090. http://dx.doi.org/10.1016/0016-7037(95)00440-8.
Sherlock, S.C., Arnaud, N.O., 1999. Flat plateau and impossible isochrons: apparent $^{40}Ar/^{39}Ar$ geochronology in a high-pressure terrain. Geochim. Cosmochim. Acta 63, 2835–2838. http://dx.doi.org/10.1016/S0016-7037(99)00116-7.
Sherlock, S.C., Kelley, S.P., 2002. Excess argon evolution in HP-LT rocks: a UVLAMP study of phengite and K-free minerals, NW Turkey. Chem. Geol. 182, 619–636. http://dx.doi.org/10.1016/S0009-2541(01)00345-X.
Sherlock, S.C., Lucks, T., Kelley, S.P., Barnicoat, A., 2005. A high resolution record of multiple diagenetic events: ultraviolet laser microprobe Ar/Ar analysis of zoned K-feldspar overgrowths. Earth Planet. Sci. Lett. 238, 329–341. http://dx.doi.org/10.1016/j.epsl.2005.07.018.
Smith, D.C., 1984. Coesite in clinopyroxene in the caledonides and its implications for geodynamics. Nature 310, 641–644. http://dx.doi.org/10.1038/310641a0.
Spencer, K.J., Hacker, B.R., Kylander-Clark, A.R.C., Andersen, T.B., Cottle, J.M., Stearns, M.A., Poletti, J.E., Seward, G.G.E., 2013. Campaign-style titanite U–Pb dating by laser-ablation ICP: implications for crustal flow, phase transformations and titanite closure. Chem. Geol. 341, 84–101. http://dx.doi.org/10.1016/j.chemgeo.2012.11.012.
Villa, I.M., 1998. Isotopic closure. Terra Nova 10, 42–47. http://dx.doi.org/10.1046/j.1365-3121.1998.00156.x.
Wain, A., 1997. New evidence for coesite in eclogite and gneisses: defining an ultrahigh-pressure province in the Western Gneiss region of Norway. Geology 25, 927–930. http://dx.doi.org/10.1130/0091-7613(1997)025<0927:NEFCIE>2.3.CO;2.
Wain, A., Waters, D.J., Jephcoat, A., Olijynk, H., 2000. The high-pressure to ultrahigh-pressure eclogite transition in the Western Gneiss Region, Norway. European Journal of Mineralogy]–>Eur. J. Mineral. 12, 667–687. http://dx.doi.org/10.1127/0935-1221/2000/0012-0667.
Walsh, E.O., Hacker, B.R., 2004. The fate of subducted continental margins: two-stage exhumation of the high-pressure to ultrahigh-pressure Western Gneiss Region, Norway. J. Metamorph. Geol. 22, 671–687. http://dx.doi.org/10.1111/j.1525-1314.2004.00541.x.
Walsh, E.O., Hacker, B.R., Gans, P.B., Grove, M., Gehrels, G., 2007. Protolith ages and exhumation histories of (ultra)high-pressure rocks across the Western Gneiss Region, Norway. Geol. Soc. Am. Bull. 119, 289–301. http://dx.doi.org/10.1130/B25817.1.
Walsh, E.O., Hacker, B.R., Gans, P.B., Wong, M.S., Andersen, T.B., 2013. Crustal exhumation of the Western Gneiss Region UHP terrane, Norway: $^{40}Ar/^{39}Ar$ thermochronology and fault-slip analysis. Tectonophysics 608, 1159–1179. http://dx.doi.org/10.1016/j.tecto.2013.06.030.
Warren, C.J., Sherlock, S.C., Kelley, S.P., 2011. Interpreting high-pressure phengite $^{40}Ar/^{39}Ar$ laserprobe ages: an example from Saih Hatat, NE Oman. Contrib. Mineral. Petrol. 161, 991–1009. http://dx.doi.org/10.1007/s00410-010-0576-1.
Warren, C.J., Kelley, S.P., Sherlock, S.C., McDonald, C.S., 2012a. Metamorphic rocks seek meaningful cooling rate: interpreting $^{40}Ar/^{39}Ar$ ages in an exhumed ultra-high pressure terrane. Lithos 155, 30–48. http://dx.doi.org/10.1016/j.lithos.2012.08.011.
Warren, C.J., Smye, A.J., Kelley, S.P., Sherlock, S.C., 2012b. Using white mica $^{40}Ar/^{39}Ar$ data as a tracer for fluid flow and permeability under high-P conditions: Tauern Window, Eastern Alps. J. Metamorph. Geol. 30, 63–80. http://dx.doi.org/10.1111/j.1525-1314.2011.00956.x.
Warren, C.J., Hanke, F., Kelley, S.P., 2012c. When can muscovite $^{40}Ar/^{39}Ar$ dating constrain the timing of metamorphic exhumation? Chem. Geol. 291, 79–86. http://dx.doi.org/10.1016/j.chemgeo.2011.09.017.
Wartho, J.A., Kelley, S.P., 2003. $^{40}Ar/^{39}Ar$ ages in mantle xenolith phlogopites: determining the ages of multiple lithospheric mantle events and diatreme ascent rates in southern Africa and Malaita, Solomon Islands. Geol. Soc. Lond., Spec. Publ. 220, 231–248. http://dx.doi.org/10.1144/GSL.SP.2003.220.01.14.
Wheeler, J., 1996. Diffarg: a program for simulating argon diffusion profiles in minerals. Comput. Geosci. 22, 919–929. http://dx.doi.org/10.1016/S0098-3004(96)00061-1.
Whitney, D.L., Evans, B.W., 2010. Abbreviations for names of rock-forming minerals. Am. Mineral. 95, 185–187. http://dx.doi.org/10.2138/am.2010.3371.
Young, D.J., Kylander-Clark, A.R.C., 2015. Does continental crust transform during eclogite facies metamorphism? J. Metamorph. Geol. 33, 331–357.
Young, D.J., Hacker, B.R., Andersen, T.B., Corfu, F., 2007. Prograde amphibolite facies to ultrahigh-pressure transition along Nordfjord, western Norway: implications for exhumation tectonics. Tectonics 26, TC1007. http://dx.doi.org/10.1029/2004TC001781.
Young, D.J., Hacker, B.R., Andersen, T.B., Gans, P.B., 2011. Structure and $^{40}Ar/^{39}Ar$ thermochronology of an ultrahigh-pressure transition in western Norway. J. Geol. Soc. 168, 887–898. http://dx.doi.org/10.1144/0016-76492010-075.